Eng. Sci., 2025, **35**, 1594

Engineered Science
DOI: https://dx.doi.org/10.30919/es1594

Fretting Wear and Corrosion in Liquid Lead-Bismuth Eutectic: A Review of Current State and Prospect

Hui Chen,[1, 2] Guiyu Mei,[1, 2] Guangzhao Wang,[1, 2] Wei Tan[1, 2] and Guorui Zhu[1, 2,*]

Abstract

Lead–bismuth eutectic (LBE) is a promising coolant for Generation-IV reactors. The corrosion of LBE and the fretting wear caused by fluid-induced vibration will gradually become the main causes of component failure. Therefore, this paper summarizes the current state of research on fretting wear in LBE. The effects of alloy composition, mechanical load, temperature and oxygen concentration on fretting wear are discussed. It also emphasizes the interaction between fretting wear and corrosion in LBE environments. Additionally, the applicability of Archard, energy dissipation and finite element modeling in LBE is evaluated, highlighting the need for corrosion-dependent calibration. Finally, the protective strategies, including aluminide coatings, ceramic coatings, high-entropy alloy coatings and cold spray layers, are also reviewed to evaluate their ability to mitigate fretting–corrosion damage. Overall, this work aims to deepen the understanding of corrosion–fretting behavior in LBE and to guide the design of more durable materials for nuclear reactors.

Keywords: Fretting wear, LBE corrosion, Wear model, Coating, Lead-cooled fast reactor.
Received: 05 May 2025; Revised: 09 Jun 2025; Accepted: 10 Jun 2025.
Article type: Research article.

1. Introduction

The history of lead-cooled fast reactors dates back to the mid-20th century when the Soviet Union developed small reactors for nuclear submarines, using lead-bismuth eutectic (LBE) as the coolant.[1] Research during this period primarily focused on reactor design, selection of alloy steels, and thermohydraulic studies. These efforts led to advancements in alloy purification and oxygen concentration control technologies.[2] However, development stalled in the late 20th century due to various technical challenges. Interest in LBE-cooled reactors was revived in the early 21st century with the rising demand for clean energy and enhanced nuclear safety. Several projects have since advanced LBE-cooled reactor technology to the experimental and demonstration stage,[3-5] including the MYRRHA program in Europe,[6] China's CLEAR series,[7,8] and the small secure transportable autonomous reactor (SSTAR) project in America,[9,10] collectively paving the way for future commercialization of lead-cooled fast reactors.

[1] *School of Chemical Engineering and Technology, Tianjin University, Tianjin, 300350, China*
[2] *Zhejiang Institute of Tianjin University, Ningbo, Zhejiang, 315201, China*
**Email:* zhuguorui@tju.edu.cn (G. Zhu)

LBE offers attractive coolant properties such as a low vapor pressure and excellent heat transfer characteristics [11,12]. These features enable high-temperature operation with minimal pressurization, contributing to inherently safe reactor behavior. However, ensuring the long-term structural integrity of reactor components exposed to the LBE environment remains crucial for safe operation. Specifically, the combined action of LBE corrosion and flow-induced fretting wear can thin or rupture heat exchanger tubes and fuel cladding, risking coolant leakage and loss of core integrity.[13,14] The compatibility between structural steels (mainly austenitic stainless steel and ferritic/martensitic steel),[15-19] and LBE has become a difficult issue in the development of new nuclear reactors.[12,20] The interplay between corrosion and fretting in LBE is especially pernicious – fretting can break or delaminate protective oxide scales, exposing fresh metal to accelerated corrosion, while corrosion can in turn reduce material strength and alter the contact conditions, exacerbating wear. Consequently, the investigation, evaluation, and prediction of fretting damage in LBE are of great importance for safety and economic issues. However, research on fretting wear in LBE remains limited. Existing studies have primarily focused on the corrosion phenomenon of nuclear steel materials in LBE and fretting wear in high-temperature and high-pressure water environments.

In light of these challenges, this paper reviews recent

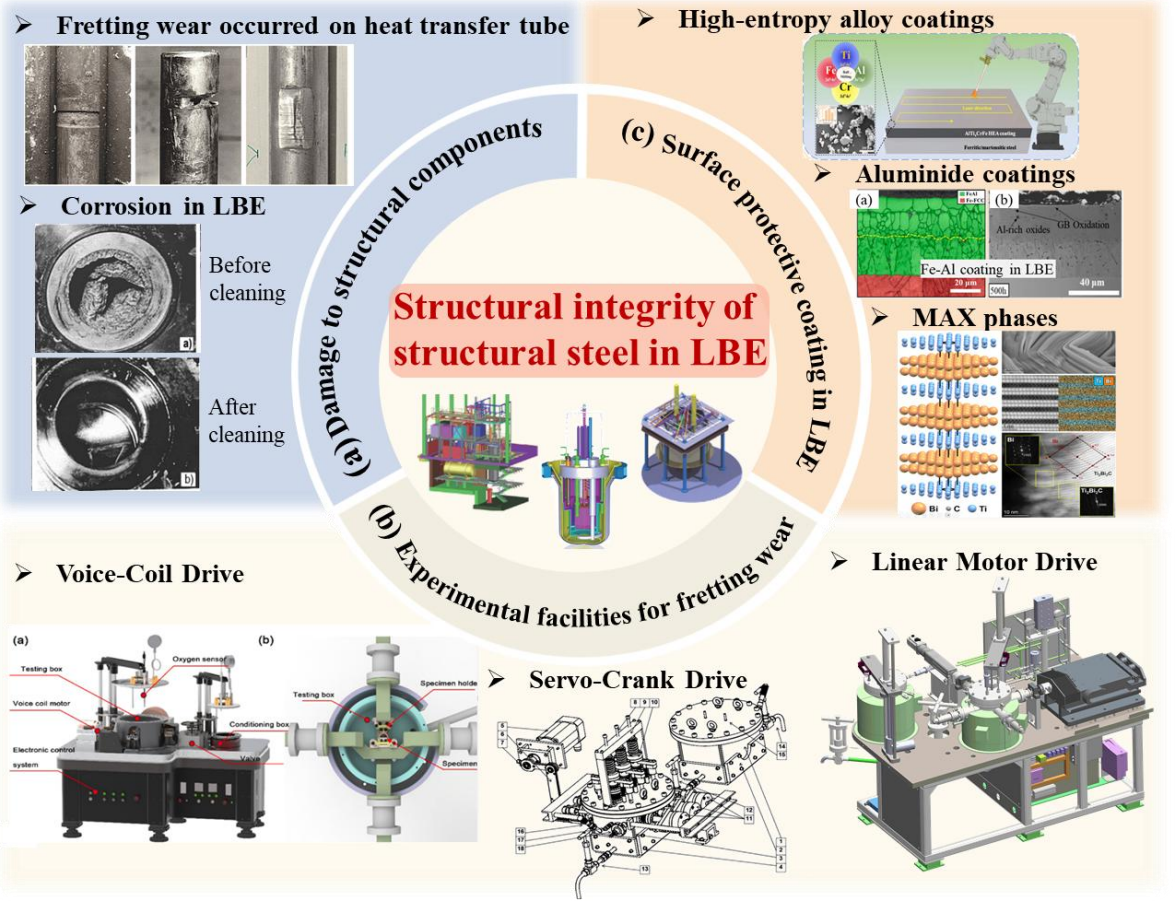

Fig. 1: Fretting wear and corrosion are unavoidable damage to structural components in a reactor. In the middle of the picture is a schematic diagram of the reactor[7] (Copyright 2016 Yican Wu). Part (a) shows an actual damage photograph in the reactor,[21,22] Copyright Ahmed Khalifa & Copyright V.M. Troyanov. To elucidate the coupled corrosion and wear mechanisms in LBE environments, multiple research groups have designed specialized test rigs. Part (b) illustrates three publicly available experimental rigs: voice-coil drive[23] (Copyright 2025 Elsevier B.V.), servo-crank drive [24] (Copyright 2012 Elsevier B.V.) and linear motor drive[25] (Copyright 2025 Elsevier B.V.). Meanwhile, numerous coating technologies have been developed. Part (c) displays the different coating types: high-entropy alloy coatings[26] (Copyright 2024 Elsevier B.V.), aluminide coatings[27] (Copyright 2024 Elsevier Ltd) and MAX-phases[28] (Copyright 2025 Elsevier Inc).

research in fretting wear of nuclear steels in LBE environments. First, this paper summarizes the corrosion behavior of common candidate alloys (primarily austenitic stainless steels and ferritic–martensitic steels) in liquid LBE, including the roles of temperature, oxygen concentration, flow conditions, and steel composition on oxidation and dissolution processes. The effects of LBE on the mechanical properties of steels are also discussed to link environmental degradation with structural integrity. Next, review research on fretting wear relevant to LBE-cooled systems, drawing implications from studies in high-temperature water and other similar conditions for LBE conditions. Following this, the progress in simulation techniques is evaluated, with an emphasis on the current limitations of these models. Finally, advanced coatings and surface treatment methods are introduced. This review aims to deepen the understanding of fretting wear in LBE-cooled reactors, thereby ensuring the safety and long-term operation of next-generation nuclear systems. Fig. 1 presents a comprehensive diagram illustrating damage, experimental rigs, and protective methods in LBE.

2 Fretting wear in LBE environments

2.1 Corrosion mechanisms in fretting damage

Structural steels in LBE environments are prone to oxidation corrosion and dissolution corrosion, which can compromise component integrity even before any mechanical wear is considered. Therefore, understanding the fundamental corrosion mechanisms in LBE is essential as a prelude to studying fretting corrosion, because the presence or absence of protective corrosion films affects the progress of fretting damage. Generally, material composition, temperature and oxygen concentration jointly determine the dominance of dissolution and oxidation corrosion.

2.1.1 Dissolution corrosion

When the oxygen content in LBE is insufficient or the alloy surface struggles to form a protective oxide film, stainless steel experiences dissolution corrosion. Alloys containing

highly soluble elements exhibit pronounced dissolution behavior. For instance, the high solubility of Ni in 316L stainless steel results in its preferential dissolution into LBE, causing material loss and surface composition alterations.[29] However, corrosion resistance can be significantly enhanced by adjusting alloy compositions, such as reducing Ni content and increasing Cr, or adding small amounts of Si, Al, or Ce. These adjustments promote the formation of stable protective oxide films.[30-32] Table 1 shows the performance comparison of various stainless steel. Despite these optimizations, severe dissolution corrosion can still occur under extremely low oxygen conditions or if protective oxide films fail to develop. Controlling oxygen content in LBE effectively mitigates dissolution corrosion. Studies indicate that when the oxygen concentration is lower than 10^{-7}wt.%, dissolution corrosion becomes dominant.[29,33-35] Fig. 2(a) shows the effect of different oxygen content in liquid lead on the corrosion transition of steels. This oxygen concentration interval has been widely recognized in liquid lead alloy. In addition to the oxygen content mentioned above, temperature is another crucial factor aggravating dissolution corrosion. When temperatures exceed approximately 550 °C, even stable Fe–Cr spinel layers on ferritic/martensitic steels such as T91 become unstable and corrosion rate increase rapidly. Numerous experimental studies highlight a temperature critical threshold, beyond which the morphology and structure of the oxide layer on the steel surface undergo significant changes,[33,34,36-39] as shown in Table 2.

Table 1: The performance comparison of different types of stainless steel.[29-39]

Steel type	Exposure condition	Characteristics	Limitations
Austenitic stainless steel (*e.g.*, 316L)	1. Oxygen concentration: 10^{-11}-10^{-3}wt.% 2. Temperature: 450 - 550 °C 3. Exposure time: 2011 - 8766 h	1. High Cr content promoting dense protective spinel oxide formation. 2. High Ni content is conducive to the stability of austenite structure.	Ni has a high solubility in LBE and is prone to selective dissolution corrosion, reducing corrosion resistance.
Modified Austenitic Stainless Steel (*e.g.*, 15-15Ti)	1. Oxygen concentration: 10^{-7}wt.% 2. Temperature: 400 °C-550 °C 3. Exposure time:288 h - 13194 h	1. Ti addition significantly improves grain boundary stability and resistance to irradiation swelling. 2. Corrosion resistance comparable to 316L in LBE environments.	High risk of selective Ni dissolution at elevated temperatures in LBE.
Ferritic/Martensitic Steel (*e.g.*, T91)	1. Oxygen concentration: 10^{-7}-10^{-3}wt.% 2. Temperature: 450 - 550 °C 3. Exposure time:8766 h and 2011 h	1. Moderate Cr content forming dense Fe-Cr spinel oxide films. 2. Low Ni content, reducing selective dissolution risk. 3. Good corrosion resistance when temperature is below 550 °C.	When temperature exceeds 550 °C, oxide film stability decreases significantly, and the corrosion resistance decreases.
New Low-activation Martensitic Steel (*e.g.*, CLAM, EUROFER)	1. Oxygen concentration: 10^{-6}wt.% 2. Temperature: 500 °C 3. Exposure time:1500 h	Optimized composition (W, Se, V, Si, etc.) and heat treatment significantly improving high-temperature mechanical properties and irradiation resistance.	1. Susceptible to dissolution corrosion under extremely low oxygen conditions. 2. Oxide film stability, long-term corrosion and fretting performance require further verification under engineering service conditions.

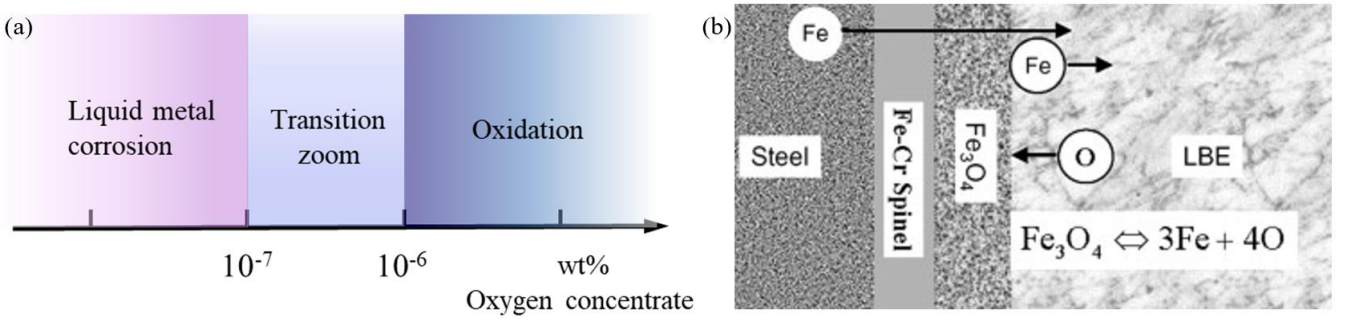

Fig. 2: (a) Relationship between corrosion form and oxygen concentration; (b) The oxidation mechanism of steel in liquid LBE,[47] Copyright 2007 Elsevier B.V.

Table 2: Oxidation layer structure of austenitic steel and ferritic/martensitic steel at different temperatures.[33,34,36-39]

	Austenitic steel	Ferritic/martensitic steel
<550 ℃	The oxide film is very thin, containing only spinel (Fe, Cr)$_3O_4$ oxide film.	Surface： Porous Fe_3O_4 Inner layer: Dense (Fe, Cr)$_3O_4$
=550 ℃	Double oxide film, possibly single layer (Fe, Cr)$_3O_4$.	Under the (Fe, Cr)$_3O_4$ layer, an inner oxide layer rich in oxygen is formed along the grain boundary.
>550 ℃	The chemical potential of O is lower than the formation energy of (Fe, Cr)$_3O_4$, the oxide film becomes unstable and prone to decomposition.	

2.1.2 Oxidation corrosion

When the oxygen concentration exceeds about 10^{-6}wt.%, a protective oxide film will rapidly form on the surface of stainless steel, making oxidation the dominant,[40] as shown in Fig. 2(a). In this form, a dense Fe–Cr oxide layer develops and significantly suppresses the dissolution of highly soluble elements into LBE.[38,41] Therefore, maintaining an optimal oxygen concentration in LBE promotes the formation of a stable and protective oxide film on nuclear steels. At present, the most widely accepted theory of oxidation mechanism is that the formation of oxide film depends on the simultaneous diffusion of anions and cations. Oxygen transport primarily occurs through micro/nano-scale Pb penetration paths within the oxide film, where oxygen initially dissolves in the LBE and subsequently diffuses along these nanoscale channels toward the metal surface, facilitating simultaneous growth of both inner and outer oxide layers,[42-46] as illustrated in Fig. 2 (b). As corrosion progresses, the oxide film may experience localized cracking due to stresses or growth defects. Once this protective film ruptures, direct contact between the liquid metal and substrate accelerates dissolution corrosion. The continuous formation and destruction of the oxide scale is therefore a critical aspect of corrosion in LBE. These microscopic mechanisms, including composition gradients caused by selective elemental dissolution, selective oxide growth under varying oxygen concentrations, and corrosion mode transitions induced by film defects or ruptures, collectively determine the corrosion behavior and rate of nuclear steels in liquid LBE. In conclusion, a stable oxide film formed under optimal conditions is the key barrier against corrosion in LBE, shifting the mechanism from dissolution to oxidation and greatly enhancing the corrosion resistance of material under fretting.

2.1.3 Synergistic fretting-corrosion effects in LBE

The presence of an oxide film plays a pivotal role in fretting scenarios, but its effectiveness depends on the corrosion mode. In oxygen-rich LBE, oxidation corrosion forms a dense oxide layer that can be protective. In oxygen-poor LBE, dissolution corrosion predominates, and alloying elements such as Ni or Cr leach directly into the melt. Fretting is characterized by small-amplitude contact between surfaces.[48] In LBE environments, fretting wear continually fractures the oxide layers formed on steel surfaces, cyclically exposing fresh metal to accelerated localized corrosion. Each time the film cracks, two paths are possible: rapid re-oxidation if oxygen is available, or direct dissolution if it is not. The protective scale therefore cannot survive long enough to shield the substrate. In effect, fretting converts a normally protective oxidation situation into a cyclic rupture scenario, forcing the steel to undergo repeated dissolution/oxidation events. Moreover, selective dissolution of alloying elements from the steel substrate leads to surface depletion and microstructural damage, reducing the hardness and fatigue strength of the surface layer.[47,49,50] A corroded steel surface is more prone to crack initiation, spalling, and wear during fretting wear. Consequently, corrosion caused by mechanical friction is different from pure oxidation or dissolution corrosion. Fretting mainly accelerates corrosion by continually stripping the already weakened surface. Corrosion and fretting act in tandem to accelerate material degradation: the oxide film cannot sustain itself under fretting and fails to prevent corrosion, while the ongoing corrosion continuously weakens the material and contributes to more severe fretting damage. This synergistic mechanism results in significantly higher wear rates and earlier failure than would be expected from corrosion or mechanical wear alone. Therefore, before analyzing the detailed fretting corrosion mechanisms in LBE, it is crucial to recognize how the fundamental corrosion processes set the stage for and influence fretting behavior.

2.2 Influencing factors on fretting wear

2.2.1 Fretting test apparatus

Before exploring the influencing factors of fretting wear,

existing devices for understanding fretting behavior in a LBE environment are shown in Fig. 3. Del Giacco *et al*.[24] designed the FRETHME apparatus, utilizing a servo motor-driven crank mechanism to generate reciprocating motions. This mechanism can achieve large displacement amplitudes. In addition, this apparatus can achieve precise oxygen control, facilitating fretting wear tests under complex environmental conditions. Using this device, the effects of displacement amplitude, normal load, and cycle number on fretting wear have been investigated. Chen *et al*.[25,51] developed a device that employs a servo motor for normal loading and a linear motor for horizontal reciprocating motion, achieving displacement control precision of 1 μm and load sensor accuracy of ±0.05%. The tube-plate line contact configuration of this apparatus allows for real-time adjustment during experiments based on sensor feedback signals. Chen *et al*. utilized this equipment to perform fretting corrosion experiments from 350 °C to 600 °C, and exploring the impacts of temperature and fretting parameters. Sun *et al*.[23] employed a device driven by a voice coil motor with a tube-tube contact configuration. Voice coil motors have the same rapid response and suitability for high-precision, small-amplitude fretting as linear ones. Their research emphasized the long-term microstructural evolution, specifically focusing on the synergistic interaction between oxide layers and wear under high-temperature conditions over extended periods. This work has compared the load control precision, displacement resolution, and temperature capability of different rigs, as shown in Table 3.

Although few fretting corrosion devices for LBE environments have been publicly disclosed, the increasing demand for deeper insights into fretting behavior under complex conditions are motivating researchers to actively develop more professional experimental equipment. These efforts aim to clarify the underlying mechanisms of corrosion-fretting wear interactions under realistic reactor operating conditions.

2.2.2 Materials

In LBE environments, the dissolution of elements such as Ni, Cr, and Fe from stainless steel leads to surface deterioration and reduces mechanical strength, making corroded surfaces more susceptible to fatigue spalling and abrasive wear under dynamic loading. Del Giacco conducted 600-hour fretting wear tests on 15-15Ti, T91, and GESA-T91 steels in LBE at 450 °C.[52] The results showed that cracks and spalling occurred on the wear surface of 15-15Ti. In contrast, GESA-T91 steel, with comparable Cr content but lower Ni, exhibited no such damage. This is because the dissolution of Ni accelerated cumulative damage, whereas the low-Ni GESA-T91 primarily lost material through oxidation and abrasive wear, exhibiting surface hardening and greater resistance to fatigue. Hua *et al*.[53] conducted fretting wear tests on 316L stainless steel after pre-immersion in LBE for different

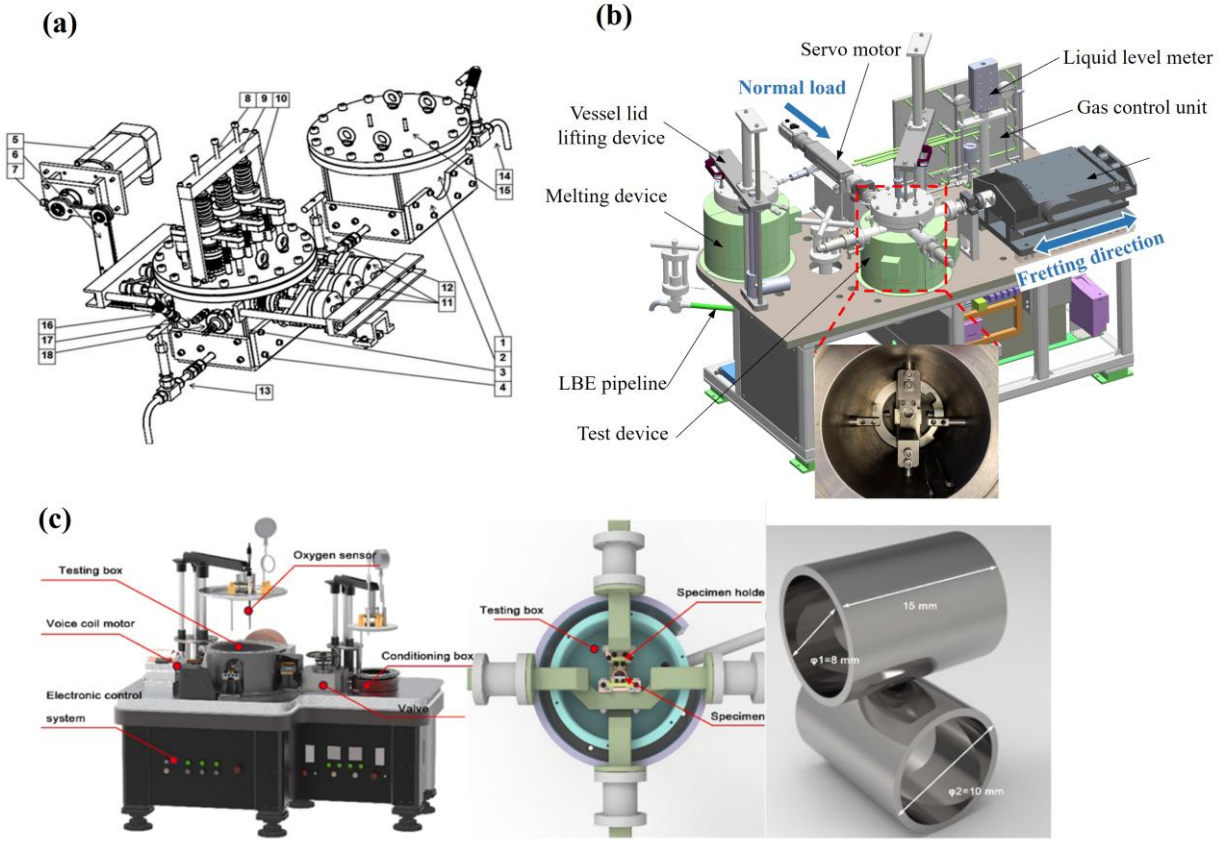

Fig. 3: The equipment developed by (a) Del Giacco[24] (Copyright 2012 Elsevier B.V.) (b) Chen,[25] (Copyright 2025 Elsevier B.V.) and (c) Sun are all capable of conducting fretting-wear tests in LBE environments.[23] (Copyright 2025 Elsevier B.V.)

durations. The results showed that short-term corrosion resulted in adhesive wear, whereas long-term corrosion caused significant Ni dissolution, deepening the wear scars and reducing wear resistance, as shown in Fig. 4. Thus, dissolution corrosion significantly reduced the wear resistance of austenitic steels, producing a synergistic acceleration of damage when combined with wear.

Additionally, alloying elements like Si and Al readily form dense protective oxide layers due to their affinity for oxygen. Cao *et al*. applied a Cr-Al-C coating on 316L stainless steel via laser cladding and analyzed the wear resistance of the coating under dynamic load conditions. The results illustrated that the wear resistance of the coating is significantly higher than that of the substrate in LBE at 320 ℃ and 450 ℃. The presence of Al-rich oxide layers effectively prevented direct substrate contact and reduced elemental dissolution.[54] SIMP steel contains higher Si content, forming denser and more corrosion-resistant oxide layers compared to T91,[55] suggesting Si mitigate oxide layer spallation.

Regarding microstructure, martensitic/ferritic steels possess a body-centered cubic (BCC) crystal structure with high hardness (300–400 HV), providing superior wear

Table 3: A comparative analysis of various fretting test rigs.

Driving Method	Displacement Range / Amplitude Accuracy	Load Range & Control Accuracy	Oxygen Control	Main Advantages	Main limitations
Servo motor + Crank mechanism (Del Giacco)	Range: 20–1000 μm. Accuracy: 2-5 μm	0–1000 N; ±1% force control	Yes	• Large amplitude and high load capability • Precise oxygen control, closely simulates reactor conditions • Proven operation at 350–550 °C	•Inertia and backlash lower accuracy at very small amplitudes or high frequencies •Motion gaps from crank pins
Servo motor loading + Linear motor reciprocation (Chen)	Range: 10–100 μm Accuracy: 0.5-1 μm	5–200 N; ±0.05% force control	No (can integrate oxygen control system)	•High displacement accuracy •Real-time feedback • Proven operation at 350–600 °C	•Linear-motor magnets need thermal isolation •Higher cost •Lack of an oxygen control system
Voice coil motor (Sun)	Range: 10–200 μm Accuracy: ≤ 0.1 μm	Small-range load; ±2% force control	No (Equipped with an oxygen sensor)	• Pure electromagnetic direct drive – no friction/backlash • High-frequency capability • Proven operation at 500 °C	• Limited amplitude and load • Higher equipment and controller cost

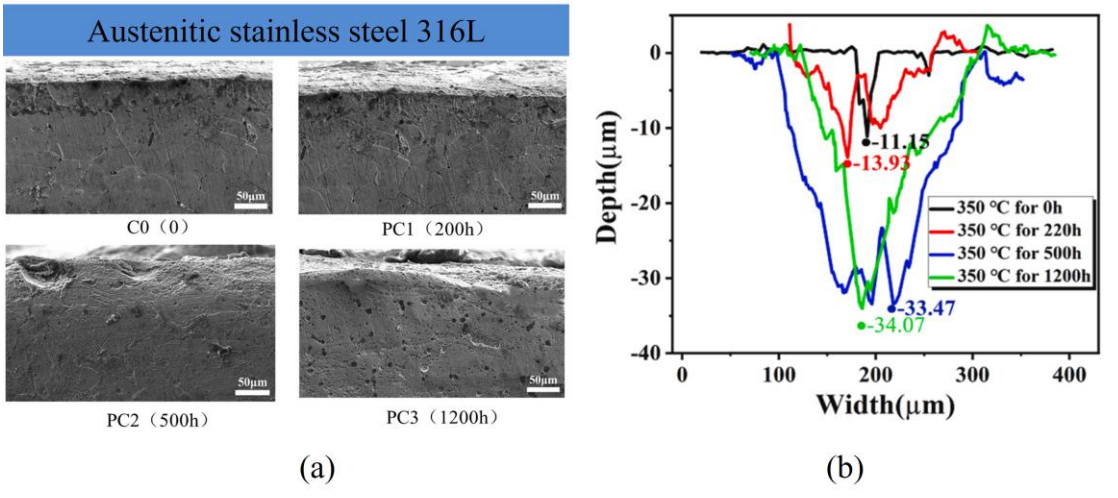

Fig. 4: (a) The SEM micrograph of the cross-section of the wear surface under 2×10^5cycles (Pre-corrosion durations: C0 none, PC1 220 h, PC2 500 h, PC3 1200 h, Pre-immersion temperature 350 ℃, Normal load 20 N, Sliding amplitude 50 μm, sliding frequency 20 Hz); (b) The wear depth for four specimen types,[53] Copyright 2022 Elsevier Ltd.

resistance under static high-stress conditions but exhibiting brittleness and susceptibility to cracking under impacts. Conversely, austenitic steels exhibit a face-centered cubic (FCC) structure, initially softer (150–200 HV), yet capable of reaching hardness above 400 HV through dislocation accumulation and strain hardening during deformation. This dynamic surface hardening improves wear resistance under fatigue and impact conditions, while their superior corrosion resistance notably enhances durability in corrosive-wear environments, resulting in better overall adaptability. In summary, the alloy composition and microstructure influence the form and stability of oxide films and corrosion products, thus determining the intensity of wear-corrosion synergy during fretting in LBE.

2.2.3 Fretting-parameters

Mechanical factors primarily include fretting frequency, displacement amplitude, and normal load.[56,57] Del Giacco *et al*. have shown how their interplay controls damage evolution. The experimental results are shown in Fig. 5. In their tests on T91 steel in liquid lead, they observed that compacted oxidized debris and debris covered on the worn surface after fretting tests. The increase in the number of cycles could lead to an increase in fretting damage at the same displacement amplitude and normal load. Moreover, the parameters demonstrated a clear threshold. Below a certain load–amplitude combination the contact operates in a mixed stick–slip regime, but once the normal load exceeds 25 N at a 35 µm amplitude, the slip regime shifts into gross slip. At larger amplitudes (75 µm and 165 µm), higher loads are required to trigger this transition.[24,52,58,59] Fu *et al*. compared the fretting wear behavior of TP316Ti stainless steel in dry and LBE environments at displacement amplitudes of 30 µm and 100 µm. The results indicated that the medium environment had no significant effect on the fretting behavior affected by fretting parameters, with friction coefficients showing similar trends.[60]

Given the observation of Fu that environmental media have minimal effects on fretting behavior, insights gained from studies conducted in water environments can be meaningfully applied to LBE conditions. Numerous experimental in water environments demonstrate that under large displacement amplitude and small load, the fretting regime tends to be the gross slip, the wear mechanism is mainly abrasive wear, and the wear degree is relatively large. Conversely, under small displacement amplitude and high normal load, the fretting regime tends to be the mixed stick and slip, and the wear mechanism is mainly adhesive and delamination. The wear degree is relatively small. Local stress and strain are relatively large, resulting in the initiation of cracks in the fretting area.[61-65] Chen *et al*.[25] investigated fretting wear of 316L stainless steel in LBE at 350°C under varying displacement amplitudes and normal loads, revealing that these two parameters jointly influenced wear mechanisms and fretting regimes, consistent

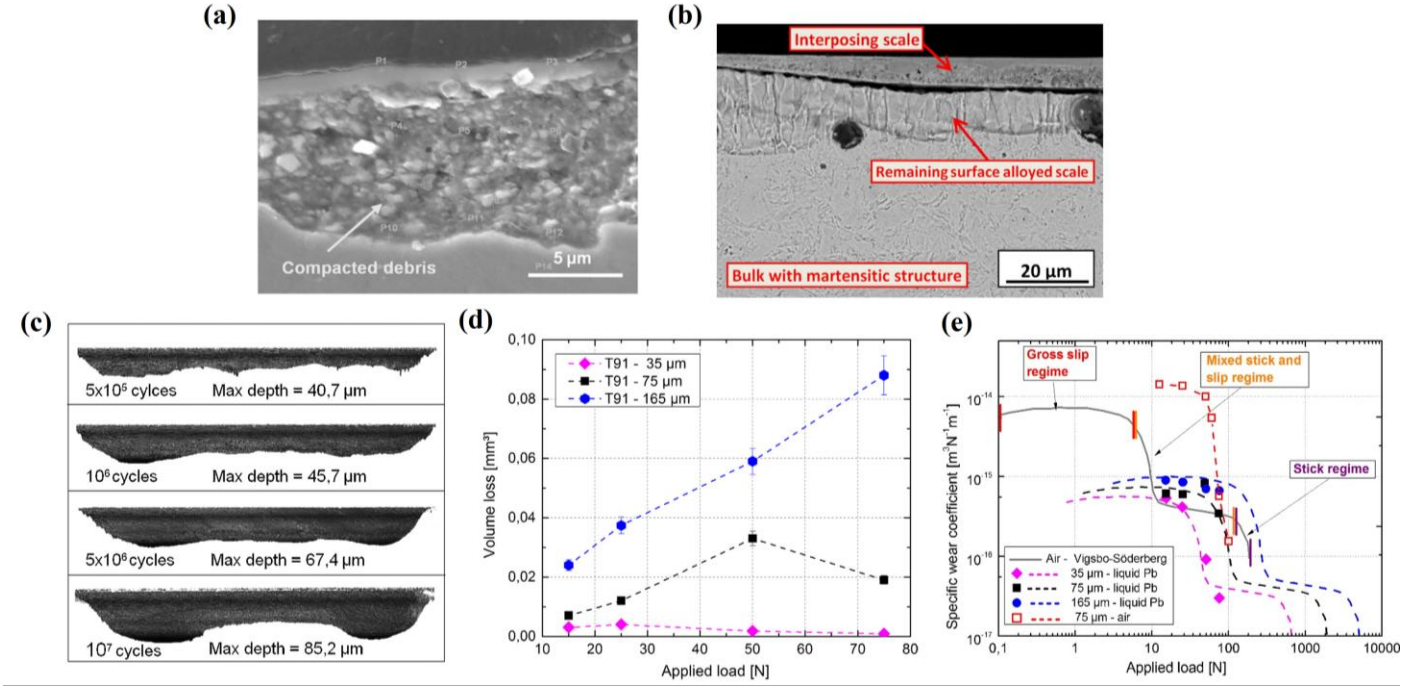

Fig. 5: (a) Cross-section of asperity formed in the fretting groove of the T91 specimen. (Test parameters: 450 °C, 50 N, 75µm),[24] Copyright 2014 Elsevier B.V. (b) SEM image in BSE mode of the fretted area of the T91 specimen. (Test parameters: 450 °C, 50 N, 75µm, 10Hz),[59] Copyright 2014 Elsevier B.V. (c) Analysis of laser profilometry cross-sections reveals changes in fretting grooves with varying numbers of cycles. (Test parameters: room temperature, 75µm, 50N, 20Hz),[24] Copyright 2012 Elsevier B.V. (d) Volume loss vs. applied load for T91. (Test parameters: 10 Hz, 150 h, 450°C,[52]) Copyright 2014 Elsevier B.V. (e) Fretting map of T91 steel (Test parameters: 450°C, 10 Hz, 150 h),[52] Copyright 2014 Elsevier B.V.

with observations in water. Nevertheless, the impact of elemental dissolution on the substrate still warrants particular attention in LBE.

In water environments, vibration-induced oxidation is frequently observed, wherein frictional heating and cyclic with observations in water. Nevertheless, the impact of elemental dissolution on the substrate still warrants particular attention in LBE. stress accelerate surface oxidation, forming thick oxide layers beneficial for reducing wear. However, the oxide layers formed is easily affected by the stress distribution and corrosion in the contact zone in LBE. Chen et al. demonstrated that debris generated in LBE at 350°C could not form stable continuous films.[25] Sun conducted long-term fretting experiments on 316L in oxygen-saturated LBE, the results revealed that corrosion damage in the contact region is significant. After 60 h of exposure, the thickness of the oxide scale at the fretting interface was 4.5 μm, while it was 0.2 μm in the unworn regions. This phenomenon indicates that crystal defects induced by high local contact stresses enhance the diffusion of oxygen atoms,[23] as shown in Fig. 6. Thus, the protective role of oxidized debris prevalent in water significantly diminishes or even disappears in LBE. Additionally, dissolution corrosion of metals, often neglected in water environments, alters surface microstructure and composition, deteriorates mechanical properties, and accelerates wear. Despite these differences, concepts from fretting studies in water environments remain applicable to LBE conditions. Firstly, the approach of dividing fretting wear regimes based on contact stress and amplitude (stick-slip and gross slip zones) remains valid in LBE, facilitating identification of mechanically or corrosion-dominated wear. Secondly, the synergistic coefficient evaluation, typically combining Archard's wear law and corrosion increments used in water, can be adapted to LBE. This framework quantitatively assesses the synergy between oxidative and dissolution corrosion contributions, providing insights into wear-corrosion interactions. For a more intuitive comparison, the publicly available wear-depth data were uniformly selected. Table 4 shows the comparison of wear depth under different experimental parameters.

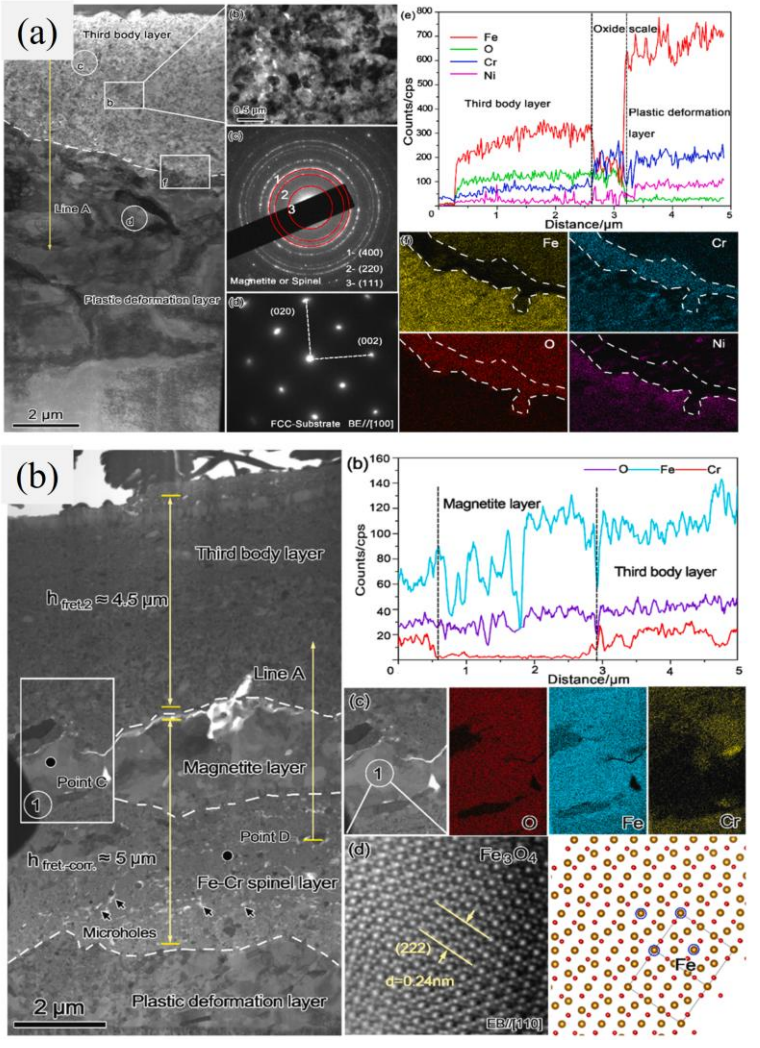

Fig. 6: (a) Microstructure of the wear zone after 20h of wear. The thickness of the oxide layer is only 0.5 μm, the damage mechanism is fretting wear, and the nickel concentration near the interface of TBL and PDL is increased, which may be the acceleration of element diffusion induced by contact stress. (b) Microstructure of the wear zone at 60h. The oxide layer is about 4.5 μm thick, and a new layer appears between TBL and PDL,[23] Copyright 2025 Elsevier.

Table 4: Comparison of wear depth under different experimental parameters in LBE.

Specimen/counter-specimen	Oxygen concentration (wt.%)	Temperature (℃)	Fretting parameters (Load, amplitude, frequency, test time)	Wear depth (μm)	Ref
1.4970/1.4970			50 N, 75 μm, 10Hz, 150 h	47	
T91/T91			50 N, 75 μm, 10Hz, 150 h	39.5	
T91/T91		450	50 N, 75 μm, 10Hz, 312 h	53	
T91/T91			50 N, 75 μm, 10Hz, 600 h	65	
T91/T91			50 N, 75 μm, 10Hz, 930 h	72	
1.4970/1.4970			50 N, 75 μm, 10Hz, 600 h	120	
1.4970/1.4970		500	50 N, 75 μm, 10Hz, 150 h	70	
T91/T91		500	50 N, 75 μm, 10Hz, 150 h	55.5	
T91/T91		550	50 N, 75 μm, 10Hz, 150 h	150	
		450	50 N, 75 μm, 10Hz, 150 h	12	[58]
	~ 10^{-6}	500	50 N, 75 μm, 10Hz, 150 h	13	[59]
GESA-T91/GESA-T91		550	50 N, 75 μm, 10Hz, 150 h	17	
		450	50 N, 75 μm, 10Hz, 312 h	17	
			50 N, 75 μm, 10Hz, 600 h	25	
			50 N, 75 μm, 10Hz, 930 h	37	
		450	50 N, 75 μm, 10Hz, 150 h	47	
		500	50 N, 75 μm, 10Hz, 150 h	70	
15-15Ti/15-15Ti		550	50 N, 75 μm, 10Hz, 150 h	85	
		450	50 N, 75 μm, 10Hz, 312 h	63	
			50 N, 75 μm, 10Hz, 600 h	90	
			50 N, 75 μm, 10Hz, 930 h	111	
316L/316L	5.5×10^{-5}	Pre-corrosion	20N, 50 μm, 10Hz, 5.6h, pre-corrosion durations 220 h	13.93	
		350	20N, 50 μm, 10Hz, 5.6 h, pre-corrosion durations 500 h	33.47	[53]
			20N, 50 μm, 10Hz, 5.6 h, pre-corrosion durations 1200 h	34.07	
T91/T91	Saturated oxygen	Pre-corrosion 500	100N, 100 μm, 5Hz, 10^5 cycles, pre-corrosion durations 1000 h	18	[66]
316L/316L	-	250	60N,40 μm, 30Hz, 18.5 h	46.8	
			60N,60 μm, 30Hz, 18.5 h	49.5	
			60N,80 μm, 30Hz, 18.5 h	52.3	
		320	60N,40 μm, 30Hz, 18.5 h	46.5	[67]
			60N,60 μm, 30Hz, 18.5 h	50.9	
			60N,80 μm, 30Hz, 18.5 h	67.6	
		450	60N,40 μm, 30Hz, 18.5 h	46.5	
			60N,60 μm, 30Hz, 18.5 h	50.2	
			60N,80 μm, 30Hz, 18.5 h	67.4	
316L/316L	Saturated oxygen	350	25N,25 μm, 20Hz, 7 h	5.4	
			25N,50 μm, 20Hz, 7 h	5.7	
			25N,75 μm, 20Hz, 7 h	7.8	
			50N,25 μm, 20Hz,7 h	3.8	
			50N,50 μm, 20Hz, 7 h	5.3	[25]
			50N,75 μm, 20Hz, 7 h	5.9	
			75N,25 μm, 20Hz, 7 h	3.4	
			75N,50 μm, 20Hz, 7h	5.3	
			75N,75 μm, 20Hz, 7h	7	
		500	20N,100 μm, 10Hz, 20 h	2.35	
			20N,100 μm, 10Hz, 60 h	6.85	[23]
			20N,100 μm, 10Hz, 100 h	11	

2.2.4 Thermal-oxygen-environment

The environment also affects fretting wear, primarily through oxygen concentration and temperature. I.V.Gorynin *et al*.[68] demonstrated that optimal oxygen concentrations range around 10^{-6} and 10^{-7} wt.%. Oxygen levels outside this range (either too high or too low) led to significantly accelerated corrosion. Fig. 2 (a) shows the relationship between different oxygen concentrations and corrosion depths in the liquid lead. Mi *et al*.[66] investigated the microstructure and fretting behavior of oxidized scales on the surface of T91 pre-exposed in saturated oxygen LBE at 500 ℃. The results showed that the oxide layer was mainly composed of a loose magnetite layer and a relatively dense Fe-Cr spinel layer, with LBE-filled holes interspersed between them. During the fretting process, the oxide film near the wear area tends to peel off layer by layer as a brittle failure mode under combined shear and normal stresses. Fig. 7 showed the damage characteristics of oxidized scales. The layers marked by arrows 1 and 2 corresponded to magnetite and spinel. The substrate can also be seen in the lower right corner. In LBE, oxygen concentration is a critical parameter, influencing oxide film formation rates, thicknesses, and structures, thus affecting wear evolution. Oxygen in LBE promotes regeneration of oxide layers on worn surfaces. In oxygen-containing LBE, a dense oxide film or a loose oxide film may form on the steel surface. The dense oxide film can prevent corrosion and fretting wear, while the loose oxide film can only prevent corrosion in the initial stage. During fretting, this brittle and loose oxide film is repeatedly cracked and spalled from the contact surfaces, continually exposing fresh metal to the liquid metal environment. Such repetitive cycles of oxidation, cracking, and regeneration significantly accelerate wear. In contrast, in an oxygen-poor LBE environment, such protective oxide debris formation is absent. The corrosion process degrades the substrate, making it easier for fretting to remove material, resulting in a higher wear rate. Therefore, the presence of oxygen significantly alters the fretting mechanism in LBE. This mechanistic understanding is critical, as it underpins later discussions on controlling oxygen and using coatings to mitigate fretting damage in LBE.

Temperature changes the characteristics of oxide films and dissolution rates of alloy elements in LBE, influencing fretting wear mechanisms. Hua *et al*.[69] studied the synergistic mechanism of fretting corrosion on 316 stainless steel in LBE, focusing on temperature effects while maintaining constant mechanical parameters. Fig. 8 shows that as the temperature increased, Ni dissolved into the liquid LBE, causing a transformation of the substrate from austenite to ferrite and a subsequent deterioration in wear resistance. The shear forces of fretting rapidly fragment the substrate, leading to rapid material removal. Furthermore, fretting wear and corrosion mutually exacerbated each other. Chen *et al*.[51] examined fretting behaviors of 316L stainless steel in LBE at various temperatures. Fig. 9 illustrated the result. They found uniform oxide film thickening at 350–450 °C, mitigating wear to some extent. However, at 600°C, the oxide structure became porous, compromising stability and significantly accelerating simultaneous wear and corrosion—a trend consistent with earlier findings by Del Giacco. Thus, temperature governs oxide film stability and elemental dissolution rates, determining whether oxidation wear or dissolution wear dominates.

From the available literature, it can be found that most of the oxygen concentrations in fretting corrosion experiments in LBE were 10^{-6} wt.%, which is thought to be the most conducive to protect the nuclear steel according to the corrosion tests. Despite extensive research by scholars on oxidation phenomena in the context of the nuclear industry, mechanistic issues such as the oxidation sequence of different elements, oxidation products, oxidation depth, and other related factors have been relatively underexplored, particularly under dynamic conditions of fretting wear in LBE. Moreover, fretting corrosion mechanisms proposed by different researchers exhibit differences. Some attribute the accelerated material loss to mechanical removal of the protective oxide layer, while others emphasize stress-assisted corrosion and dissolution processes as dominant factors. The comparability of experimental data is difficult due to

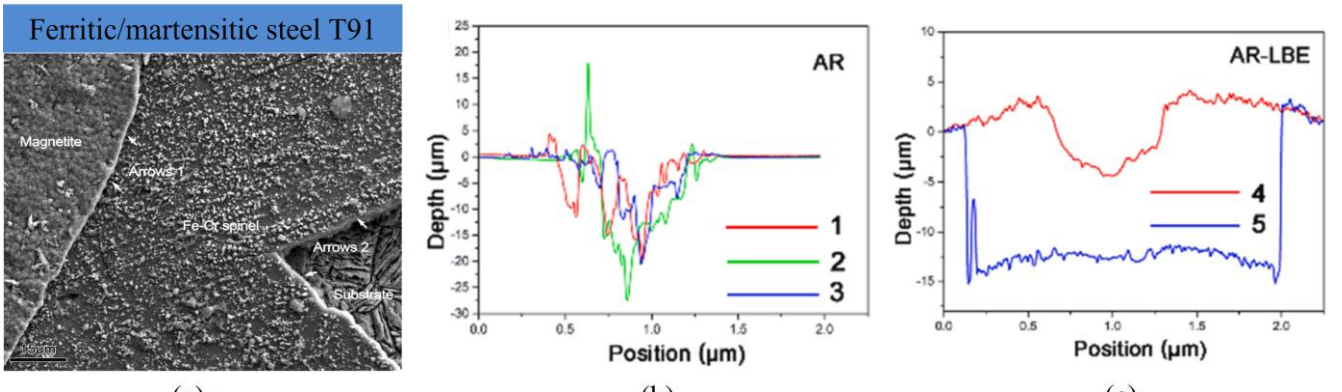

Fig. 7: (a) The SEM image exhibits the damaged feature of oxide scales close to the worn region (Displacement amplitude 100 μm, normal forces 100 N, frequency 5 Hz, 10^5 cycles). (b) and (c) were wear profiles of different specimen in AR (without LBE) and AR-LBE (in LBE),[66] Copyright 2023 Elsevier Ltd.

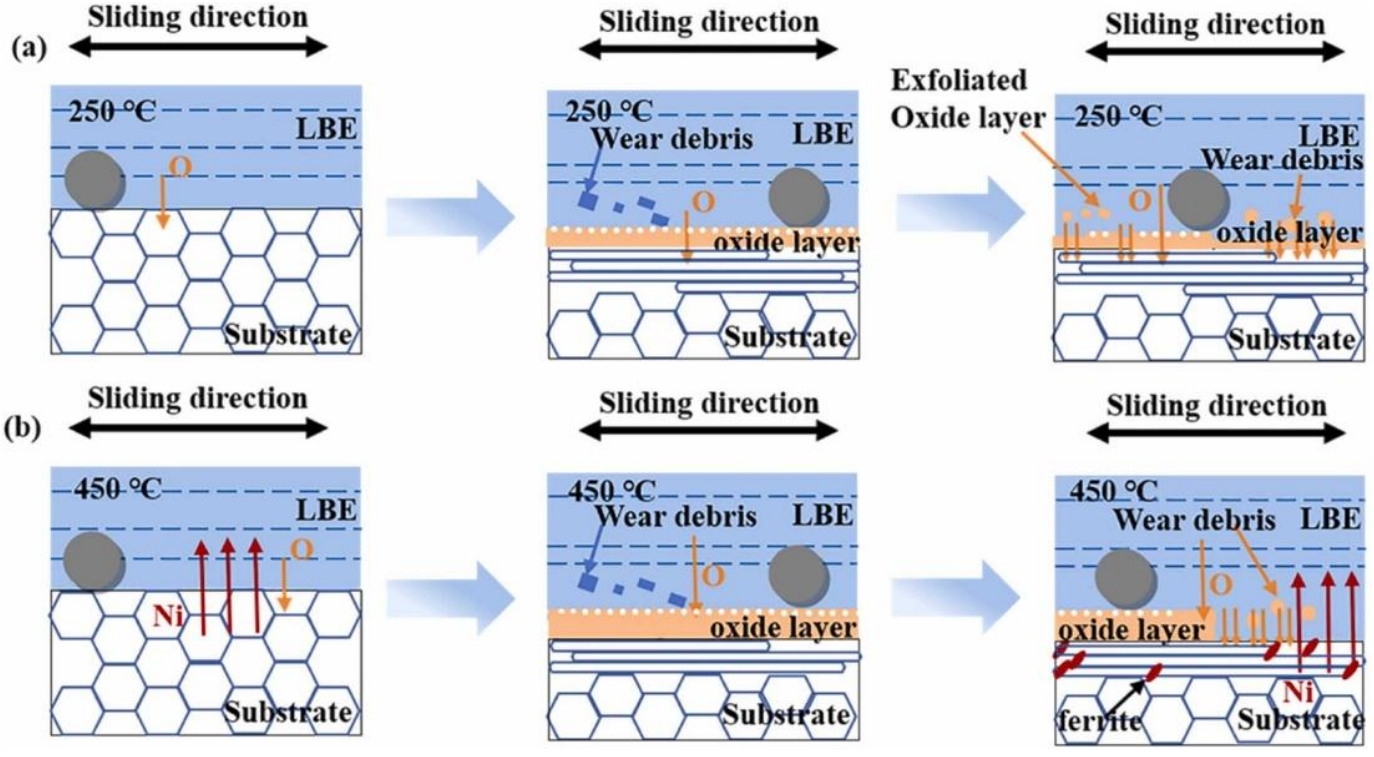

Fig. 8: Schematic diagrams depict the fretting corrosion damage observed on 316 stainless steel in LBE at distinct temperatures: (a) 250 °C and (b) 450 °C.[69] (Displacement amplitude 80 μm, normal forces 60 N, frequency 30 Hz, 2×10^6 cycles), Copyright 2023 Elsevier Ltd.

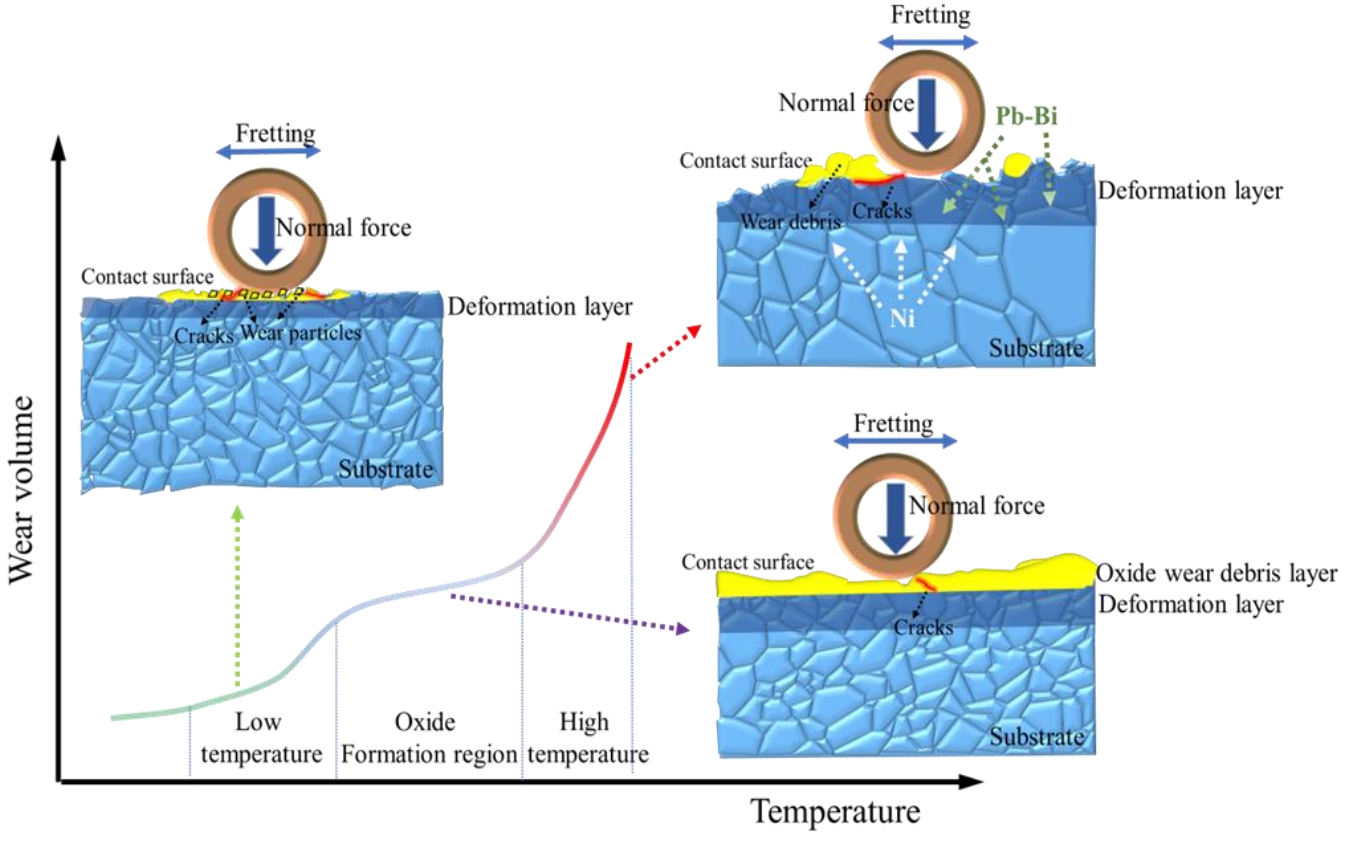

Fig. 9: Fretting wear failure mechanisms at different temperatures.[51] (Displacement amplitude 75 μm, normal forces 50 N, frequency 20 Hz, 1×10^5 cycles), Copyright 2025 Elsevier B.V.

variations in experimental parameters and conditions. Therefore, establishing a standardized fretting-corrosion protocol is essential for conducting more systematic and mechanistic investigations in the future. The correlation between oxidative corrosion, dissolution corrosion, and wear warrants greater attention. Future studies on oxygen levels and temperature in LBE will clarify fretting-corrosion mechanisms and guide new material design.

2.3 Discussion on the applicability of fretting wear models in LBE environment

Selecting an appropriate wear model is crucial for accurately predicting the fretting wear behavior of nuclear stainless steels in LBE environments. Currently, common approaches include the Archard model, energy consumption model, and various mathematical model. However, due to the unique corrosion characteristics and oxide growth processes in LBE, traditional models require suitable modifications to ensure applicability. With advancements in computational methods, increasing numbers of researchers employ finite element methods (FEM) and machine learning models to investigate relationships between wear volume and multiple physical parameters.

2.3.1 Archard wear model

The Archard wear model is a classic quantitative wear model proposed in the 1950s, the wear volume can be calculated as shown in Eq. (1).[70,71] It is defined that wear starts when asperities on smooth surfaces meet. Local stress at the contact points causes plastic deformation, generating wear particles after a certain sliding distance. The particles are considered to be equiaxial in shape. The Archard wear model reflects that the wear volume of a material is directly proportional to the normal load and sliding distance, and is inversely proportional to the material hardness. Fig. 10 presents a simplified model diagram of wear.

$$V = KFS \tag{1}$$

where V is the wear volume, m^3, K is the wear coefficient, $m^3 \cdot N^{-1} \cdot m^{-1}$ or Pa^{-1}, F is the normal load, N, S is the sliding distance, m.

After the Archard wear model was proposed, it was quickly applied to the study of fretting wear.[72,73] In this model, the friction coefficient between the contact surfaces is defined as a constant and is only applicable to the gross slip conditions. Additionally, the Archard model is typically applied to dry friction or low-corrosion environments, and its predictive accuracy can be significantly affected by corrosive or oxidative conditions. To address these issues, Fallahnezhad *et al* studied the fretting wear under corrosion conditions and introduced the corrosion layer thickness into the Archard model.[74] By coupling the Archard wear equation with an electrochemical model describing regenerated oxide layers, they conducted finite element simulations using the UMESHMOTION subroutine in ABAQUS (Abaqus Unified Finite Element Analysis) to predict wear depth and volume under corrosive conditions. Although the method targets water environments, it still provides valuable insights for the LBE environment. In LBE environments, the Archard model can serve as a baseline to estimate mechanical wear volumes. However, adjustments to the wear coefficient are required to account for corrosion effects. Dissolution and oxidation caused by LBE produce a significant wear-corrosion synergy, enhancing material degradation beyond mechanical wear alone. Consequently, while the Archard model remains useful for predicting baseline wear due to vibration or contact in LBE, the wear coefficient must be corrected through experiments to accurately reflect corrosion-induced material loss.

2.3.2 Energy dissipation model

The energy dissipation model was proposed in the 1960s. Mohrbacher *et al*.[75-77] found that in the state of fretting contact, energy dissipation is proportional to the wear volume. Fouvry *et al*.[78-80] conducted further research on this phenomenon and defined the relationship between fretting wear and energy dissipation. The equation is as follows:[80]

$$\mathrm{V} = \alpha E_d \tag{2}$$

where V is the wear volume, m^3, α is the energy dissipation method wear coefficient m^3/J, E_d is the total wear energy consumption, J.

$$E_d = \int Q \, dS \tag{3}$$

where Q is the shear friction force, N, S is the sample displacement amplitude, m.

Due to significant energy transformations associated with oxide film formation and rupture in corrosive environments, energy-based wear models are particularly suitable for evaluating the protective effects of oxide films and wear-corrosion synergy. Fouvry *et al*.[81] conducted finite element analysis of fretting wear on Ti-6Al-4V based on the the cylinder/plate model and introduced the concept of energy wear. Guo *et al*.[82,83] incorporated energy loss into the Archard

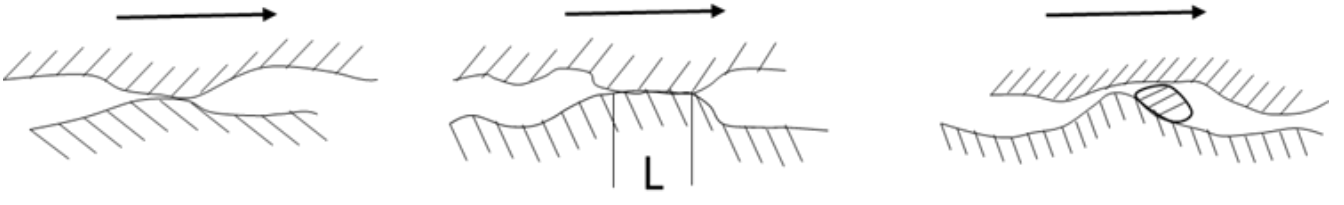

Fig. 10: Archard model diagram.

wear model demonstrating improved accuracy in predicting wear volume, as shown in Fig. 11. Pan *et al*.[84] proposed an improved energy wear model to study the fretting wear dynamics behaviors of 3D ball-plane contact structures, and verified the model through wear experiments. The shape of wear profiles and wear depth under different slip regimes are obtained from the simulation results. These studies highlight a clear correlation between energy dissipation and oxide film breakdown-regeneration during wear processes. Although direct application of energy-based models to the LBE environment is not extensively documented, studies conducted in other corrosive conditions suggest that chemically induced energy consumption can similarly be incorporated into energy models. This approach offers a physically meaningful framework for evaluating wear-corrosion interactions and a valuable insight for wear prediction in LBE environments.

Compared to the Archard wear model, the wear coefficient in the energy dissipation model is not affected by the displacement amplitude and the friction coefficient, but it needs to obtain a large amount of friction force-displacement data, and the energy value is obtained by integration. The energy dissipation model provides a more dynamic approach to predicting fretting wear. The reliance of this model on energy dissipation aligns closely with the physical interactions occurring at the contact surfaces, providing a robust framework for understanding and predicting wear behavior under various conditions. The integration of this model with finite element analysis tools like ABAQUS enhances its practical applicability, providing more information for the design and maintenance of components subjected to fretting wear.

In summary, the energy dissipation model offers a sophisticated method for analyzing fretting wear. It avoids some limitations of the Archard model by focusing on energy parameters rather than pure mechanical ones. This shift towards energy-based modeling represents a significant step forward in the accurate prediction and management of wear in engineering applications.

2.3.3 Other mathematical models

The development of finite element methods has provided a powerful tool for studying fretting wear. By embedding the Archard wear model within finite element iterations, it is possible to simulate evolving contact surface morphologies during wear. For example, Huang corrected the M-B fractal contact model by simplifying the contact of two rough surfaces into an ideal rigid contact surface and one rough contact surface.[85] The contact deformation of the rough surface was divided into complete elastic deformation, elastoplastic deformation, and complete plastic deformation. The critical contact area function and the average contact pressure relation of asperities under different deformations were obtained, enabling numerical analysis of tangential fretting wear based on the rough surface. Huang's model focuses on the deformation behavior of rough surfaces, offering a detailed breakdown of contact mechanics. Li *et al*. further employed the ABAQUS UMESHMOTION subroutine in finite element simulations to study fretting wear on rough surfaces under different normal loads.[86,87] Fig. 12 (a) shows the finite element model, and Fig. 12 (b) illustrates the results under different parameters. Although traditional Finite Element Method (FEM) wear simulations require substantial computational resources due to fine meshes and frequent remapping, optimizations such as adaptive step sizes can enhance computational efficiency by two orders of magnitude. Currently, most FEM-based studies focus on purely mechanical fretting wear. Fortunately, these approaches can be readily extended to liquid LBE environments. By introducing corrosion-film growth and rupture criteria or evolving wear coefficients over time, finite element model can predict material thinning and lifetime under long-term LBE exposure. The advancement of machine learning has introduced data-driven methods to predict material wear and corrosion behaviors. Given the complexity and multiplicity of wear-influencing factors, data-driven models can capture nonlinear relationships from large experimental datasets, providing reliable wear and corrosion rate predictions. Luo *et al*.[88] constructed the characteristic value of wear debris and took

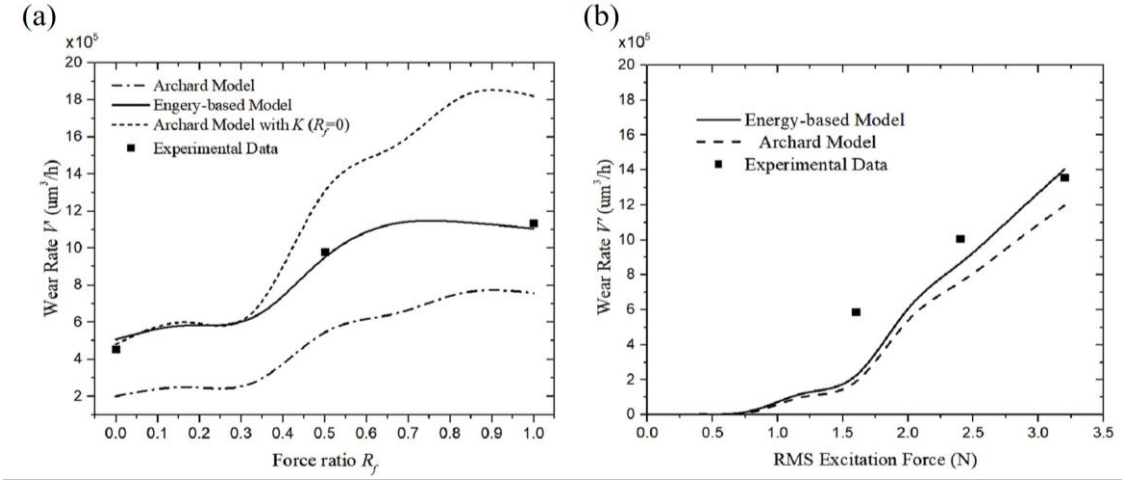

Fig. 11: Wear rate comparison between the experimental data and predicted data.[82] Copyright 2020 Elsevier Ltd.

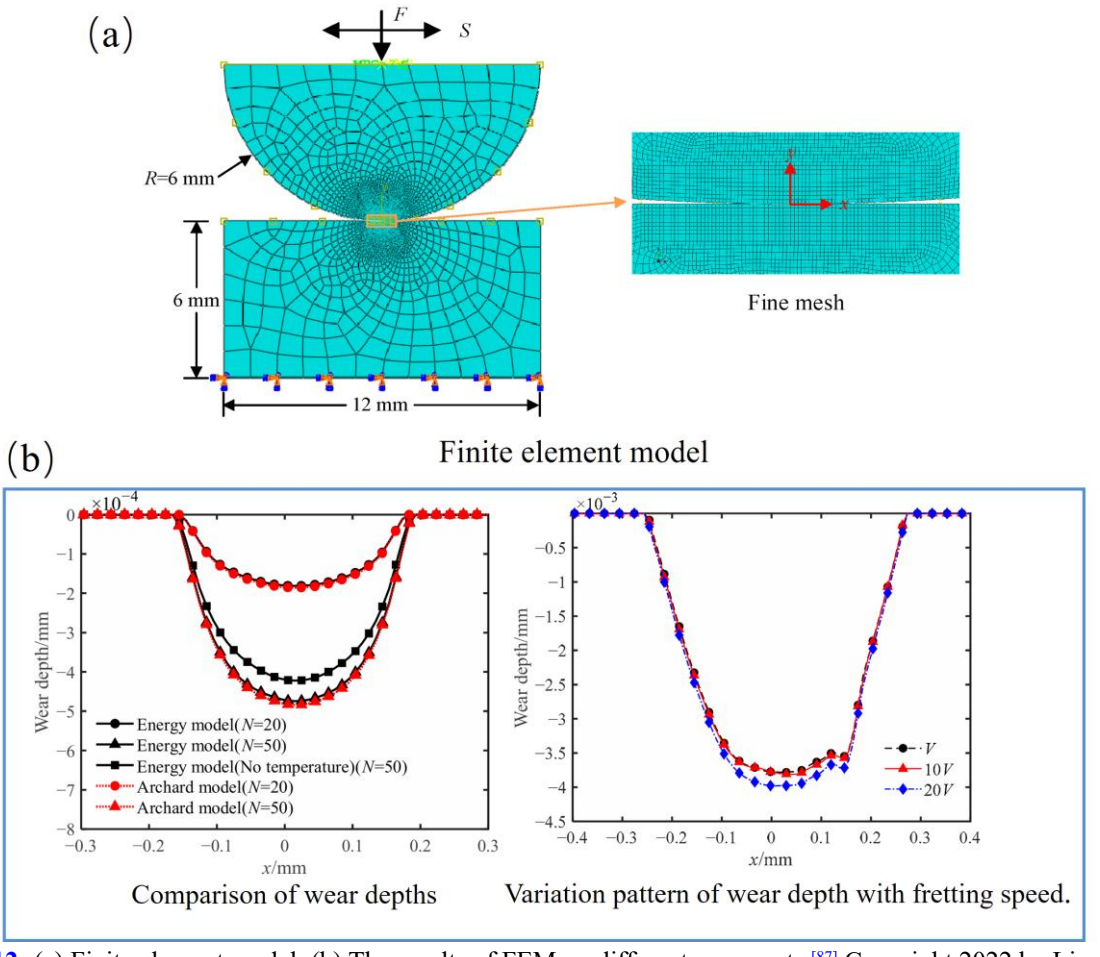

Fig. 12: (a) Finite element model; (b) The results of FEM on different paraments,[87] Copyright 2022 by Ling Li.

the wear debris value as input and contact resistance as output. The Backpropagation (BP) neural network was used to train data, achieving predictive capabilities. Zhang *et al.*[89] constructed comprehensive parameters pv (product of contact stress and fretting velocity) and pvt (product of pv value and fretting time) to express the influence of contact load, fretting amplitude, fretting time, and frequency on the fretting wear of wire rope. Zhang's comprehensive parameters provide a straightforward method to quantify multiple influencing factors. These studies demonstrate the feasibility and value of data-driven models for predicting wear and corrosion in liquid metal environments. When sufficient experimental data exist, artificial neural network (ANN) models can rapidly forecast corrosion-wear behaviors under varied conditions to assess service life. Moreover, machine learning combined with finite element simulations can generate artificial datasets, expanding the training data when experimental results are limited. However, neural network accuracy depends heavily on the training data range. Thus, extrapolation beyond existing data must be done cautiously. Overall, data-driven methods like neural networks offer promising solutions for predicting complex wear-corrosion phenomena in LBE environments.

Furthermore, physically based wear models also provide valuable insights. For example, P.h. Hipway *et al.* proposed that wear rate depends on the slowest among three processes: oxygen ingress into the contact area, oxide debris generation, and debris removal. Hipway's physical-based wear rate equation emphasizes the importance of material and environmental interactions in wear processes. Therefore, the wear rate equation was proposed from the physical point of view. Fig. 13 shows the variation of rate process with the increase of energy dissipation. Wear is modeled by three competing processes with the slowest (the rate-determining process) setting the overall wear rate. The summary of the competing rate equations is as follow:[90]

$$\text{Regime I (Archard wear)}\ \left(\frac{dV}{dE}\right)_{\mathrm{I}} = A \tag{4}$$

$$\text{Regime II (Oxygen transport)}\ \left(\frac{dV}{dE}\right)_{\mathrm{II}} = B\frac{C_{atm}D}{\delta^{*}\mu P f b^{2}} \tag{5}$$

$$\text{Regime III (Debris ejection)}\ \left(\frac{dV}{dE}\right)_{\mathrm{III}} = \frac{G\beta}{\mu b} \tag{6}$$

where A (with S.I. units of $m^3\ J^{-1}$), B (with S.I. units of $m^6\ kg^{-1}$), G (with S.I. units of $m^4\ J^{-1}$) are empirical constants; V is the wear volume; E is the energy dissipated; C_{atm} is the oxygen concentration in the atmosphere; D represents the effective diffusion coefficient governing oxygen transport across the interface region; δ^* is the slip amplitude; μ is the coefficient of friction; P is the normal load; f is the fretting frequency; and

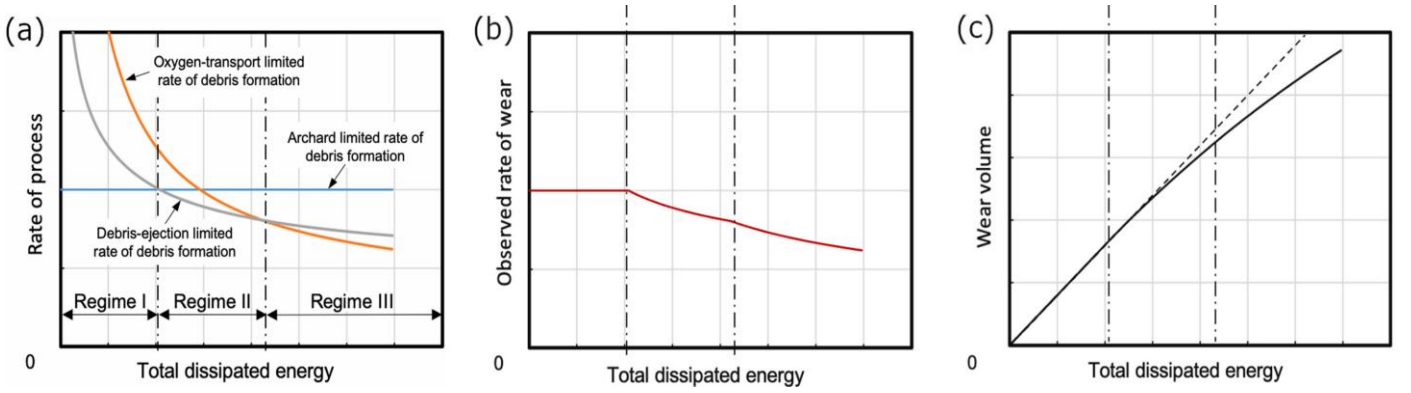

Fig. 13: (a) The variation of rate process with energy dissipation. The variation of (b) observed wear rate and (c) total wear volume with energy dissipation,[90] Copyright 2021 Elsevier B.V.

b is the contact semi-width; β denotes the proportion of the slip amplitude that debris particles travel during each cycle.

These additional mathematical models provide various perspectives and methods for analyzing fretting wear. A comparative table detailing inputs, outputs, predictive accuracy, computational complexity, and the extent of corrosion consideration for Archard, energy-based, FEM, and ML models has been incorporated in Table 5. The integration of these models enhances the understanding and prediction of fretting wear by incorporating different aspects of the wear process, including surface deformation and environmental effects. This offers a more comprehensive approach to addressing wear in engineering applications.

3. Protective coatings in LBE environments

Ensuring the safe and stable operation of critical components in fourth-generation nuclear reactors and accelerator-driven systems (ADS) necessitates enhancing corrosion and wear resistance of metallic materials. Selecting appropriate surface protection strategies requires comprehensive consideration of corrosion conditions, wear modes, and process feasibility. This section summarizes several current surface modification techniques, including aluminide coatings, ceramic coatings, metallic alloy coatings, cold spraying technology, and self-forming oxide films. In addition, their protective effects, underlying mechanisms, and potential engineering applications on stainless steels are evaluated.

Table 5: Comparison of wear models used for fretting corrosion in LBE.

Model category	Key input parameters	Main outputs	Typical Prediction error	Computational effort	Treatment of corrosion
Archard wear model	Load; Amplitude; Wear coefficient	Cumulative wear volume or depth	Highly sensitive to the calibrated K value and test regime.	Low	Not explicit, corrosion is only 'hidden' inside the calibrated K value
Energy dissipation model	Dissipated frictional energy; Wear coefficient	Cumulative wear volume or depth	Usually tracks experimental trends but still shows noticeable scatter.	Low–moderate (energy integral)	Corrosion not explicit; All ΔE converted to mechanical damage
Finite-element simulation	Elastic–plastic material data; Contact geometry; Friction coefficient	Wear depth; Stress/strain map; Time-dependent profile evolution	Good agreement when properly calibrated.	High (re-meshing or UMESHMOTION sub-routine)	Can incorporate corrosion by adding oxide-growth / dissolution sub-models or reducing material properties locally
Machine-learning	Load; Amplitude; Frequency; Temperature; Oxygen level; Material	Wear rate, lifetime	High fidelity within the training domain.	Medium–high (model training phase; fast inference)	Can capture corrosion influence if corrosion-related features are included in the training set

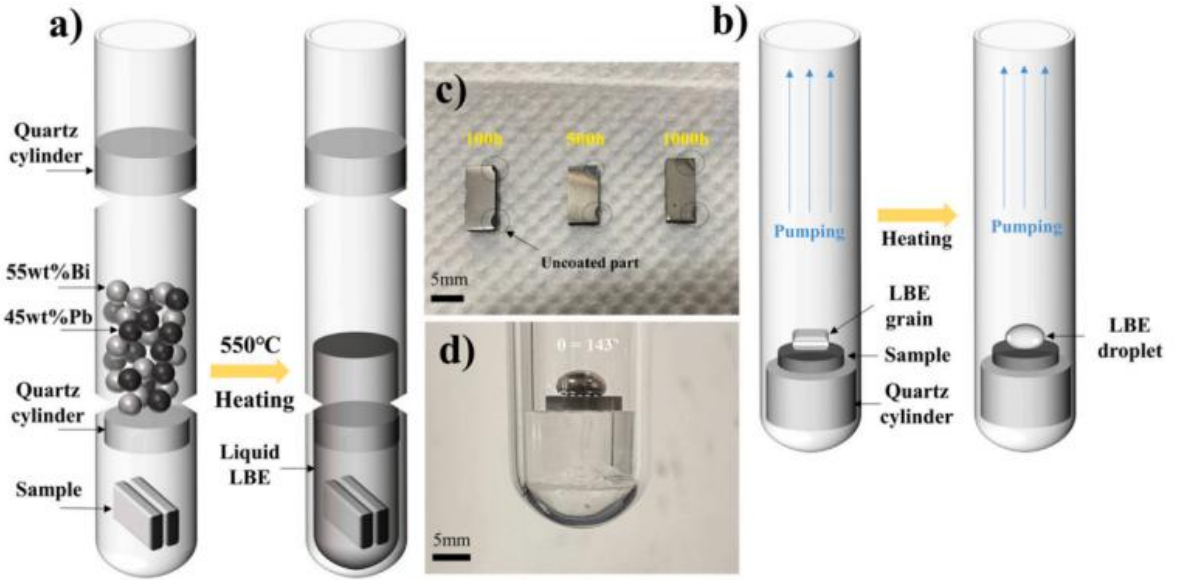

Fig. 14: (a) Corrosion test; (b) Schematic diagram of the wettability test apparatus; (c) Photos of the Al_2O_3 coating after the corrosion test; (d) Contact Angle of liquid LBE on the surface of the Al_2O_3 coating,[91] Copyright 2022 Elsevier B.V.

Aluminide coatings, typically produced via aluminizing diffusion or slurry coating methods, form Fe-Al compounds on steel surfaces. The core mechanism exploits the low Gibbs free energy of aluminium oxidation, promoting the formation of stable and dense Al_2O_3 protective films that isolate the substrate from LBE. Wen *et al*. prepared Fe-Al coatings on 316LN stainless steel via aluminizing,[27] observing minimal substrate corrosion after 1500-hour exposure at 550 °C in both oxygen-poor and oxygen-rich environments. The coating maintained its original thickness, and its structure remained intact. Zhong *et al*. used magnetron sputtering to deposit an amorphous–nanocrystalline Al_2O_3 coating on F/M steel.[91] Fig. 14 outlines the corrosion test. The uncoated steel corroded severely, reaching a depth of 24 μm after 1000 h. In contrast, the low-wettability Al_2O_3 layer blocked Pb-Bi penetration and showed excellent corrosion resistance. Aluminide coatings also resist corrosion in LBE. However, their protective oxide films can repeatedly fracture and regenerate during wear, potentially affecting coating-substrate adhesion. Further validation is thus necessary under combined corrosion-wear conditions.

Ceramic coatings, characterized by high hardness and chemical inertness, represent another route to enhance corrosion and wear resistance. Common ceramic coatings include carbides (TiC), nitrides (TiN, AlTiN), oxide ceramics, and MAX phases. Glasbrenner coated T91 steel with TiN+2–3%Cr (CVD), CrN+W (PVD),[92] and DLC, showing no corrosion failure in long-term static and dynamic LBE exposures. Particularly, TiN coating retained strong adhesion and stress-corrosion resistance even under applied static stress. MAX phases, layered ceramics with metal-ceramic hybrid properties, form protective oxide layers enhancing corrosion resistance. Rui *et al*. reported Ti_3SiC_2 surface roughening and oxide transition layer formation after short-term LBE corrosion at 450 °C,[93] indicating strong corrosion resistance to liquid Pb and Pb-Bi eutectics. The oxidation layer near the matrix side tended to be stable in 450 °C LBE for 500 h, the thickness is about 0.62 μm. However, inherent ceramic brittleness poses risks of cracking and spallation under cyclic stress. Cao *et al*. prepared a Cr_2AlC coating on a 316L substrate using laser cladding.[54] Fretting wear tests in LBE showed that the coating had significantly better wear resistance than the substrate. The coating formed a protective layer that slows down wear, as shown in Fig. 15 (a) and (b). At 450 °C, the wear resistance of the coating was 33 times higher than that of the substrate. Miorin *et al*. applied two Al-rich coatings on T91: a TiAlN layer by High Power Impulse Magnetron Sputtering (HiPIMS) and an Al-O layer by Radio Frequency Magnetron Sputtering (RFMS).[94] After 1200 h in static LBE at 550 °C, both coatings remained smooth and showed excellent corrosion resistance. The TiAlN coating also provided superior wear resistance compared with the Al-O layer, as shown in Fig. 15 (f) and (g).

Metal alloy coatings incorporate corrosion-resistant elements (Al, Cr, Y) to resist LBE-induced corrosion through formation of dense oxide films. FeCrAl and FeCrAlY coatings, widely researched and technologically mature, have demonstrated reliable protection under diverse conditions. In the early stage, Weisenburger remelted FeCrAlY coating by an electron pulse of Gas Electron Surface Alloying (GESA) to homogenize the coating.[95] The results showed that no corrosion phenomenon was observed in the LBE environment with high-speed flow. The flow rate had little effect on the coating, and the stable alumina layer morphology remained relatively intact. Li et al. used plasma spraying and laser cladding to deposit FeCrAlY-Al_2O_3 coatings, as shown in Fig. 15 (c) and (d). The results showed that the increase in Al content gradually refined the grain size of the coating.

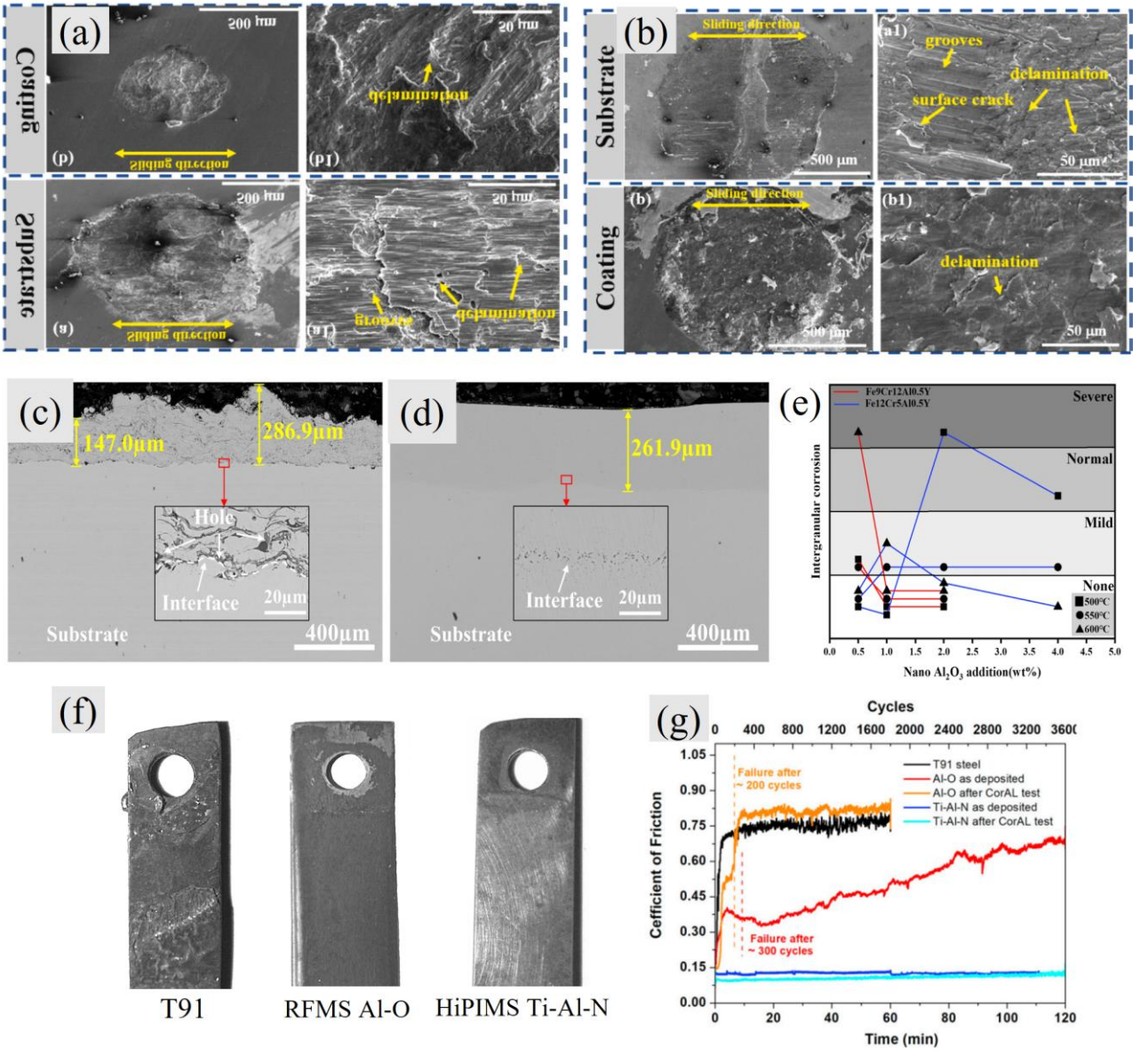

Fig. 15: SEM microstructure of wear scars of coating and substrate after fretting wear at (a) 320 ℃ and (b) 450 ℃.[54] Copyright 2024 Elsevier Ltd. SEM cross-sectional images of $Fe_{12}Cr_5Al_{0.5}Y$ (1 wt% Al_2O_3) coating after (c) plasma spraying and (d) laser remelting; (e) Diagram of degree of intergranular corrosion in liquid LBE.[96] Copyright 2024 Elsevier Ltd. (f) Picture of corrosion in 550 ℃ LBE for 1200 hours; (g) The relationship between the coefficient of friction and the number of cycles.[94] Copyright 2019 Elsevier B.V.

Appropriate Al content significantly affected the corrosion resistance of the coating in LBE. At 600 °C for 1000 h, the Fe12Cr5Al0.5Y coating with 1 wt % nano-Al_2O_3 showed the best corrosion resistance, retaining an Al-rich oxide film < 1 μm thick and limiting intergranular attack to ≤ 2 μm, as shown in Fig. 15(e).[96] Zhang *et al*. optimized FeCrAlY coatings, significantly reducing corrosion rates compared to bare T91 steel. High-entropy alloy (HEA) coatings, combining multiple metals,[97] can form complex oxide films with superior high-temperature stability and present a recent emerging direction. Yang *et al*. found that an AlCrFeMoTi HEA coating in LBE produced a thin, dense oxide layer with minimal element loss at 550 °C and 650 °C.[98] The thickness loss of the coating was only 0.5 μm and 1.0 μm after static LBE corrosion for 1000 h. However, at 650 °C, it developed localized oxidation, element segregation, and interfacial porosity. Despite good oxidation and irradiation resistance, its adhesion and long-term stability still need further assessment.[99]

Cold spraying is a low-temperature, high-velocity deposition process that directly deposits metal or alloy particles in the solid state onto a substrate, forming a coating with controllable thickness. This technique provides a new approach for on-site preparation of protective coatings and is especially suitable for repairing large or complex components. Its major advantage lies in avoiding high temperatures, thus preventing degradation of the microstructure and mechanical

Table 6: Comparison of protective coatings.

Coating type	Deposition method	Compatible substrates	Performance in LBE	Main failure mechanisms
Al diffusion coating	Slurry aluminizing	T91, 316 and similar steels	Little change in the coating thickness after 1500 h in 550 °C LBE, while corrosion depth is 60 μm for un-coated substrate.[28]	Al depletion and oxide-scale spallation during very long high-temperature exposure
Ceramic coating	Flame spray	SIMP/ CLAM steel	Good corrosion resistant with no LBE penetration in 550 °C static LBE for 300 h.[98]	LBE corrosion seriously affect the smoothness of contact surface.
High-entropy alloy nitride coating	Magnetron co-sputtering	F/M steel	Forms dense Cr–Fe spinel, mass gain < 1 mg/cm² after 1000 h in saturated O_2 LBE at 450–550 °C.[100]	Thermal-expansion mismatch with substrate may lead to interfacial stress cracking
Cold-spray	Solid-state cold spraying	Stainless steels	Deposited Cr-coating significantly improved surface wettability compared to the Zircaloy-4 substrate.[101] This method has application prospects in LBE.	Porosity or locally unbonded regions can trigger pitting or local corrosion over long service times

properties of substrate. However, if the particle interfaces formed during cold spraying are not fully metallurgically bonded, they may serve as initiation sites for fatigue cracks.

Self-forming oxide films, by controlling dissolved oxygen in LBE cooling loops, provide economically viable corrosion protection. However, fretting significantly diminishes the protective effect, mechanically rupturing oxide layers. Therefore, self-forming oxide films are often coupled with other coating methods for robust, long-term protection.

In conclusion, addressing corrosion and fretting wear challenges in LBE demands targeted selection and integration of multiple surface engineering techniques. Table 6 presents the performance comparison of different coatings in LBE. Future engineering applications may adopt combined "coating plus oxygen control" strategies, such as anti-corrosion coatings with controlled oxygen environments ensuring continuously regenerating oxide films. Alloy or composite coatings with enhanced toughness are preferable in high-vibration regions, complemented by vibration-reducing designs if necessary. Currently, aluminide and FeCrAl-based coatings are closest to practical application in future LBE-cooled reactors and ADS systems. Ceramic and HEA coatings offer higher performance potential but require further development in process reliability. Mature surface modification technologies will significantly enhance the longevity of heat exchanger tubes, reduce maintenance costs, and address material barriers for the practical deployment of LBE-cooled nuclear systems.

4. Conclusion and prospects

Corrosion and fretting wear in liquid lead-bismuth eutectic (LBE) significantly impact the integrity and safety of Generation IV lead-cooled fast reactors. Key findings highlight compatibility issues of structural steels with LBE due to factors like temperature, alloy composition, and oxygen concentration. Protective oxide films offer limited protection due to mechanical disruption during operation. Fretting wear driven by coolant-induced vibration is another critical factor, though current mechanistic understanding remains qualitative.

Advancements in modeling fretting-corrosion interactions using finite element methods and machine learning are promising but require validation through experimental data. Similarly, advanced protective coatings (such as cold spraying, aluminide coatings, ceramics, laser cladding) demonstrate substantial corrosion and wear resistance. However, their stability and lifetime under dynamic conditions must be clarified.

To further advance our understanding regarding fretting-corrosion interactions in LBE, future research directions should address:

(1) In-depth mechanistic studies: The study of fretting wear in nuclear steel within liquid LBE is currently inadequate. To explore the interaction between corrosion and fretting wear on the damage mechanism and properties of metal, more extensive experimentation is needed to understand the influencing factors, including high temperatures above 550 °C, dynamic oxygen control, new materials, a wider range of normal loads and fretting amplitude, etc. Future work should identify key factors influencing the synergy between wear and corrosion.

(2) Impact wear during reactor operation: During actual operation, nuclear reactor equipment experiences axial and lateral flow of high-speed coolant, leading to impact wear. It is crucial to focus more on the role of impact wear in conjunction with fretting wear.

(3) Model and simulation improvements: Current wear models predominantly output wear volume and wear depth, neglecting aspects such as the transformation of wear mechanisms, changes in material hardness and properties in the wear contact region, variations in wear debris, and the effect of corrosion. Simultaneously, the experimental environments used in these models are often overly simplistic. Therefore, fretting wear models should be extended to include both wear and corrosion. Enhanced models must be validated through detailed experimental data to refine predictive capabilities essential for reactor safety and maintenance

planning.

(4) Protective coating optimization: Design and evaluate new wear- resistant and corrosion-resistant coatings such as high-entropy alloys and gradient-functional coatings. Compare their long-term performance in liquid LBE and clarify primary failure mechanisms for practical application.

In conclusion, the synergistic effect of corrosion and fretting wear in LBE significantly influences material integrity and reactor safety in Generation IV lead-cooled systems. Continued research focusing on the identified gaps and proposed directions will not only fill the current void in understanding but also provide the tools and technologies, which ensure the structural integrity of next-generation nuclear reactors over decades of operation. Such progress is pivotal for the future deployment of sustainable nuclear energy systems with enhanced safety and economic performance.

Acknowledgments

This work is supported by the National Key Research and Development Program of Ningbo (2024Z096) and the Youth Talent Program of China National Nuclear Corporation.

Conflict of Interest

There is no conflict of interest.

Supporting Information

Not applicable.

References

[1] A. Alemberti, The lead fast reactor: an opportunity for the future? *Engineering*, 2016, **2**, 59-62, doi: 10.1016/J.ENG.2016.01.022.

[2] Y. Kurata, M. Futakawa, S. Saito, Corrosion behavior of steels in liquid lead–bismuth with low oxygen concentrations, *Journal of Nuclear Materials*, 2008, **373**, 164-178, doi: 10.1016/j.jnucmat.2007.05.051.

[3] L. Mansani, A. Alemberti, L. Mansani, M. Frogheri, E. Bubelis, M. Schikorr. ELFR: The European Lead Fast Reactor. Design, Safety Approach and Safety Characteristics, Proceedings of the Technical Meeting on Impact of Fukushima Event on Current & Future Fast Reactor Designs. Dresden, Germany, 19-23 March 2012.

[4] Y. Wu, Y. Bai, Y. Song, Q. Huang, Z. Zhao, L. Hu, Development strategy and conceptual design of China lead-based research reactor, *Annals of Nuclear Energy*, 2016, **87**, 511-516, doi: 10.1016/j.anucene.2015.08.015.

[5] M. Tarantino, M. Angiolini, S. Bassini, S. Cataldo, C. Ciantelli, C. Cristalli, A. Del Nevo, I. Di Piazza, D. Diamanti, M. Eboli, A. Fiore, G. Grasso, F. Lodi, P. Lorusso, R. Marinari, D. Martelli, F. Papa, C. Sartorio, M. Utili, A. Venturini, Overview on lead-cooled fast reactor design and related technologies development in ENEA, *Energies*, 2021, **14**, 5157, doi: 10.3390/en14165157.

[6] P. Baeten, M. Schyns, R. Fernandez, D. De Bruyn, G. Van den Eynde, MYRRHA: a multipurpose nuclear research facility, *EPJ Web of Conferences*, 2014, **79**, 03001, doi: 10.1051/epjconf/20137903001.

[7] Y. Wu, Design and R&D progress of China lead-based reactor for ADS research facility, *Engineering*, 2016, **2**, 124-131, doi: 10.1016/J.ENG.2016.01.023.

[8] M. Y. Ali, M. Jin, G. Zhang, L. Wang, Numerical analysis of thermal stratification dependence on mass flow rate of coolant during LOFA in pools of CLEAR-S, *Progress in Nuclear Energy*, 2020, **125**, 103380, doi: 10.1016/j.pnucene.2020.103380.

[9] A. Alemberti, V. Smirnov, C. F. Smith, M. Takahashi, Overview of lead-cooled fast reactor activities, *Progress in Nuclear Energy*, 2014, **77**, 300-307, doi: 10.1016/j.pnucene.2013.11.011.

[10] C. F. Smith, W. G. Halsey, N. W. Brown, J. J. Sienicki, A. Moisseytsev, D. C. Wade, SSTAR: The US lead-cooled fast reactor (LFR), *Journal of Nuclear Materials*, 2008, **376**, 255-259, doi: 10.1016/j.jnucmat.2008.02.049.

[11] B. Chalmers, Metals reference book Edited by C. J. Smithells. Second edition, 1955. Butterworths Scientific Publications, London; Interscience Publishers Inc., New York. 2 volumes; Price: £8 8s; $25, *Acta Metallurgica*, 1956, **4**, 230, doi: 10.1016/0001-6160(56)90155-9.

[12] J. Zhang, A review of steel corrosion by liquid lead and lead–bismuth, *Corrosion Science*, 2009, **51**, 1207-1227, doi: 10.1016/j.corsci.2009.03.013.

[13] S. S. Hwang, C. Namgung, M. K. Jung, H. P. Kim, J. S. Kim, Rupture pressure of wear degraded alloy 600 steam generator tubings, *Journal of Nuclear Materials*, 2008, **373**, 71-74, doi: 10.1016/j.jnucmat.2007.05.020.

[14] X. Guo, P. Lai, L. Tang, J. Lu, J. Wang, L. Zhang, Fretting wear of alloy 690 tube mated with different materials in high temperature water, *Wear*, 2018, **400**, 119-126, doi: 10.1016/j.wear.2018.01.001.

[15] X. Gong, R. Li, M. Sun, Q. Ren, T. Liu, M. P. Short, Opportunities for the LWR ATF materials development program to contribute to the LBE-cooled ADS materials qualification program, *Journal of Nuclear Materials*, 2016, **482**, 218-228, doi: 10.1016/j.jnucmat.2016.10.012.

[16] X. Liu, Y. Miao, M. Li, M. A. Kirk, S. A. Maloy, J. F. Stubbins, Ion-irradiation-induced microstructural modifications in ferritic/martensitic steel T91, *Journal of Nuclear Materials*, 2017, **490**, 305-316, doi: 10.1016/j.jnucmat.2017.04.047.

[17] G. Gupta, Z. Jiao, A. N. Ham, J. T. Busby, G. S. Was, Microstructural evolution of proton irradiated T91, *Journal of Nuclear Materials*, 2006, **351**, 162-173, doi: 10.1016/j.jnucmat.2006.02.028.

[18] I. Serre, J.-B. Vogt, Mechanical properties of a 316L/T91 weld joint tested in lead–bismuth liquid, *Materials & Design*, 2009, **30**, 3776-3783, doi: 10.1016/j.matdes.2009.01.038.

[19] L. Medina-Almazán, T. Auger, D. Gorse, Liquid metal embrittlement of an austenitic 316L type and a ferritic–martensitic T91 type steel by mercury, *Journal of Nuclear Materials*, 2008, **376**, 312-316, doi: 10.1016/j.jnucmat.2008.02.032.

[20] M. Kondo, M. Takahashi, N. Sawada, K. Hata, Corrosion of steels in lead-bismuth flow, *Journal of Nuclear Science and Technology*, 2006, **43**, 107-116, doi: 10.1080/18811248.2006.9711073.

[21] K. Ahmed. Fluidelastic Instability in Heat Exchanger Tube Arrays. PhD thesis, McMaster University, Hamilton, Canada, 2012.

[22] V. M. Troyanov, G. I. Toshinsky, V. S. Stepanov, V. V. Petrochenko, Lead-bismuth cooled reactors: history and the potential of development. part 1. history of development, *Nuclear Energy and Technology*, 2022, **8**, 187-195, doi: 10.3897/nucet.8.93908.

[23] Q. Sun, Y. Qin, X. Fan, Y. Liang, X. Mi, M. Zhu, Insight into the fretting corrosion behavior of 316L steel in liquid lead-bismuth eutectic at 500 ℃, *Journal of Nuclear Materials*, 2025, **603**, 155448, doi: 10.1016/j.jnucmat.2024.155448.

[24] M. Del Giacco, A. Weisenburger, P. Spieler, F. Zimmermann, F. Lang, J. A., G. Mueller, Experimental equipment for fretting corrosion simulation in heavy liquid metals for nuclear applications, *Wear*, 2012, **280**, 46-53, doi: 10.1016/j.wear.2012.01.018.

[25] H. Chen, W. Pei, S. Zhang, W. Tan, G. Zhu, A study on the fretting corrosion of 316L in static lead-bismuth eutectic (LBE): The role of slip amplitude and normal force on damage mechanism at 350 ℃, *Journal of Nuclear Materials*, 2025, **603**, 155466, doi: 10.1016/j.jnucmat.2024.155466.

[26] P. Zhang, Z. Yao, S. Lin, Y. Liu, S. Lu, X. Wu, Enhancing LBE corrosion resistance through inhibition diffusion approach for $AlTi_xCrFe$ HEA coating, *Applied Surface Science*, 2024, **669**, 160535, doi: 10.1016/j.apsusc.2024.160535.

[27] W. Wang, Z. Zhu, L. Yang, J. Lu, J. Huang, J. Tan, W. Kuang, Superior corrosion resistance of a slurry FeAl coating on 316LN stainless steel in 550 ℃ liquid lead-bismuth eutectic, *Corrosion Science*, 2024, **227**, 111757, doi: 10.1016/j.corsci.2023.111757.

[28] Y. Kushnir, B. Ratzker, M. Dahlqvist, M. Baranov, B. Favelukis, A. Nitsan, N. Maman, A. Upcher, V. Ezersky, J. Rosen, M. Sokol, Expanding MAX phases: Discovery of a double-A-layer Ti_2Bi_2C with rhombohedral symmetry, *Matter*, 2025, 102152, doi: 10.1016/j.matt.2025.102152.

[29] E. L. Maia, A. Tsybanev, S. Gavrilov, V. Tsisar, J. Lim, I. De Graeve, Oxygen-enhanced dissolution corrosion of austenitic stainless steel 316 L in static lead-bismuth eutectic at 500 ℃, *Corrosion Science*, 2024, **236**, 112224, doi: 10.1016/j.corsci.2024.112224.

[30] V. Tsisar, C. Schroer, O. Wedemeyer, A. Skrypnik, J. Konys, Asme. Corrosion of 9% Cr ferritic/martensitic steels in flowing Pb-Bi eutectic with 10-7 mass% dissolved oxygen at 450 and 550 ℃, Proceedings of the 24th International Conference on Nuclear Engineering. Charlotte, North Carolina, USA, 2016.

[31] W. Luo, Q. Huang, L. Luo, Z. Xiao, J. Wei, H. Cao, Effect of minor addition of Ce on microstructure and LBE corrosion resistance for CLAM steel, *Corrosion Science*, 2022, **209**, 110796, doi: 10.1016/j.corsci.2022.110796.

[32] Y. Gao, M. Takahashi, M. Nomura, Experimental study on diffusion of Ni in lead-bismuth eutectic (LBE), *Energy Procedia*, 2015, **71**, 313-319, doi: 10.1016/j.egypro.2014.11.884.

[33] V. Tsisar, C. Schroer, O. Wedemeyer, A. Skrypnik, J. Konys, Long-term corrosion of austenitic steels in flowing LBE at 400 ℃ and 10−7 mass% dissolved oxygen in comparison with 450 and 550 ℃, *Journal of Nuclear Materials*, 2016, **468**, 305-312, doi: 10.1016/j.jnucmat.2015.09.027.

[34] K. Lambrinou, E. Charalampopoulou, T. Van der Donck, R. Delville, D. Schryvers, Dissolution corrosion of 316L austenitic stainless steels in contact with static liquid lead-bismuth eutectic (LBE) at 500 ℃, *Journal of Nuclear Materials*, 2017, **490**, 9-27, doi: 10.1016/j.jnucmat.2017.04.004.

[35] Y.-F. Wang, J.-S. Li, W. Xu, X.-Z. Wang, Oxidation and dissolution behavior of FeCrNiAl based high entropy alloy and alumina-forming austenitic steel exposed to lead-bismuth eutectic (LBE), *Corrosion Science*, 2024, **227**, 111693, doi: 10.1016/j.corsci.2023.111693.

[36] C. Fazio, G. Benamati, C. Martini, G. Palombarini, Compatibility tests on steels in molten lead and lead–bismuth, *Journal of Nuclear Materials*, 2001, **296**, 243-248, doi: 10.1016/S0022-3115(01)00538-4.

[37] G. Chen, N. Ju, Y. Lei, D. Wang, Q. Zhu, T. Li, Corrosion behavior of 410 stainless steel in flowing lead-bismuth eutectic alloy at 550 ℃, *Journal of Nuclear Materials*, 2019, **522**, 168-183, doi: 10.1016/j.jnucmat.2019.05.029.

[38] O. Yeliseyeva, V. Tsisar, G. Benamati, Influence of temperature on the interaction mode of T91 and AISI 316L steels with Pb–Bi melt saturated by oxygen, *Corrosion Science*, 2008, **50**, 1672-1683, doi: 10.1016/j.corsci.2008.02.006.

[39] V. Tsisar, C. Schroer, O. Wedemeyer, A. Skrypnik, J. Konys, Corrosion behavior of austenitic steels 1.4970, 316L and 1.4571 in flowing LBE at 450 and 550℃ with 10−7 mass% dissolved oxygen, *Journal of Nuclear Materials*, 2014, **454**, 332-342, doi: 10.1016/j.jnucmat.2014.08.024.

[40] I. V. Gorynin, G. P. Karzov, V. G. Markov, V. A. Yakovlev, Structural materials for atomic reactors with liquid metal heat-

transfer agents in the form of lead or lead: Bismuth alloy, *Metal Science and Heat Treatment*, 1999, **41**, 384-388, doi: 10.1007/BF02469876.

[41] G. Müller, G. Schumacher, F. Zimmermann, Investigation on oxygen controlled liquid lead corrosion of surface treated steels, *Journal of Nuclear Materials*, 2000, **278**, 85-95, doi: 10.1016/S0022-3115(99)00211-1.

[42] M. Kieser, H. Muscher, A. Weisenburger, A. Heinzel, G. Müller, Liquid metal corrosion/erosion investigations of structure materials in lead cooled systems: Part 1, *Journal of Nuclear Materials*, 2009, **392**, 405-412, doi: 10.1016/j.jnucmat.2008.12.327.

[43] I. V. Gorynin, G. P. Karzov, V. G. Markov, V. A. Yakovlev, Structural materials for atomic reactors with liquid metal heat-transfer agents in the form of lead or lead: Bismuth alloy, *Metal Science and Heat Treatment*, 1999, **41**, 384-388, doi: 10.1007/BF02469876.

[44] E. Yamaki, K. Ginestar, L. Martinelli, Dissolution mechanism of 316L in lead–bismuth eutectic at 500°C, *Corrosion Science*, 2011, **53**, 3075-3085, doi: 10.1016/j.corsci.2011.05.031.

[45] G. Ilinčev, D. Kárník, M. Paulovič, A. Doubková, The effect of temperature and oxygen content on the flowing liquid metal corrosion of structural steels in the Pb–Bi eutectic, *Nuclear Engineering and Design*, 2006, **236**, 1909-1921, doi: 10.1016/j.nucengdes.2006.02.003.

[46] M. Zhang, G. He, M. Lapington, W. Zhou, M. P. Short, P. A. J. Bagot, F. Hofmann, M. P. Moody, Nano-scale corrosion mechanism of T91 steel in static lead-bismuth eutectic: a combined APT, EBSD, and STEM investigation, *Acta Materialia*, 2024, **271**, 119883, doi: 10.1016/j.actamat.2024.119883.

[47] J. Zhang, N. Li, Review of the studies on fundamental issues in LBE corrosion, *Journal of Nuclear Materials*, 2008, **373**, 351-377, doi: 10.1016/j.jnucmat.2007.06.019.

[48] S. R. Soria, S. Claramonte, A. Yawny, Evolution of fretting wear with the number of cycles on Inconel 690 steam generator tubes against AISI 420 steel under gross slip conditions, *Tribology International*, 2021, **155**, 106803, doi: 10.1016/j.triboint.2020.106803.

[49] T. Alden, D. A. Stevenson, J. Wulff. Solubility of Nickel and Chromium in Molten Lead. *Transactions of the Metallurgical Society of AIME*, 1958, **212**, 15–17.

[50] J. R. WEEKS, A.J. ROMANO. Liquidus Curves and Corrosion of Fe, Ti, Zr, and Cu in Liquid Bi-Pb Alloys. *Corrosion Science*, 1969, **25**, 131-136.

[51] H. Chen, Z. Feng, G. Mei, W. Tan, G. Zhu, The role of lead-bismuth eutectic temperature in affecting fretting corrosion of 316L stainless steel, *Wear*, 2025, **572**, 205997, doi: 10.1016/j.wear.2025.205997.

[52] M. Del Giacco, A. Weisenburger, G. Müller, Fretting of fuel cladding materials for Pb cooled fast reactors: Approach to long term prediction using fretting maps, *Nuclear Engineering and Design*, 2014, **280**, 697-703, doi: 10.1016/j.nucengdes.2014.05.043.

[53] K. Hua, Y. Cao, X. Yu, Q. Huang, Y. Tong, Y. Wang, F. Zhang, H. Wu, X. Wang, H. Wang, Investigation on fretting wear mechanism of 316 stainless steel induced by Ni dissolution during pre-immersion corrosion in the liquid lead-bismuth eutectic (LBE), *Tribology International*, 2022, **174**, 107772, doi: 10.1016/j.triboint.2022.107772.

[54] Y. Cao, K. Hua, L. Sun, H. Ding, H. Wu, H. Wang, Revealing fretting wear resistance mechanism under liquid lead-bismuth eutectic of Cr-Al-C composite coatings fabricated by laser cladding, *Tribology International*, 2024, **198**, 109898, doi: 10.1016/j.triboint.2024.109898.

[55] H. Zhang, X. Liu, Y. Xu, L. Zhao, T. Peng, C. Qin, R. Yu, Z. Wang, C. Yao, Comparison investigation on corrosion of SIMP and T91 steels exposed to liquid LBE at 450 °C: The role of Si on reducing oxidation rate, *Corrosion Science*, 2023, **225**, 111553, doi: 10.1016/j.corsci.2023.111553.

[56] X. Guo, P. Lai, L. Li, L. Tang, L. Zhang, Progress in studying the fretting wear/corrosion of nuclear steam generator tubes, *Annals of Nuclear Energy*, 2020, **144**, 107556, doi: 10.1016/j.anucene.2020.107556.

[57] Z. R. Zhou, S. R. Gu, L. Vincent, An investigation of the fretting wear of two aluminium alloys, *Tribology International*, 1997, **30**, 1-7, doi: 10.1016/0301-679x(95)00118-n.

[58] M. Del Giacco, A. Weisenburger, G. Mueller, Fretting corrosion in liquid lead of structural steels for lead-cooled nuclear systems: Preliminary study of the influence of temperature and time, *Journal of Nuclear Materials*, 2012, **423**, 79-86, doi: 10.1016/j.jnucmat.2012.01.007.

[59] M. Del Giacco, A. Weisenburger, G. Mueller, Fretting corrosion of steels for lead alloys cooled ADS, *Journal of Nuclear Materials*, 2014, **450**, 225-236, doi: 10.1016/j.jnucmat.2013.07.005.

[60] F. Jiangwen, H. Jifan, L. Jianhua, P. Jinfang, Z. Minhao. Fretting Wear Mechanism of TP316Ti in High Temperature Dry Condition and Liquid Lead-Bismuth Environments. *Tribology*, 2024, 1-19, doi:10.16078/j.tribology.2024057.

[61] I. R. McColl, J. Ding, S. B. Leen, Finite element simulation and experimental validation of fretting wear, *Wear*, 2004, **256**, 1114-1127, doi: 10.1016/j.wear.2003.07.001.

[62] H. Mohrbacher, J. P. Celis, J. R. Roos, Laboratory testing of displacement and load induced fretting, *Tribology International*, 1995, **28**, 269-278, doi: 10.1016/0301-679X(95)00005-O.

[63] N. Ohmae, T. Tsukizoe, The effect of slip amplitude on fretting, *Wear*, 1974, **27**, 281-294, doi: 10.1016/0043-1648(74)90114-8.

[64] N. J. Fisher, A. B. Chow, M. K. Weckwerth, Experimental fretting-wear studies of steam GeneratorMaterials, *Journal of Pressure Vessel Technology*, 1995, **117**, 312-320, doi: 10.1115/1.2842129.

[65] S. Söderberg, U. Bryggman, T. McCullough, Frequency effects in fretting wear, *Wear*, 1986, **110**, 19-34, doi: 10.1016/0043-1648(86)90149-3.

[66] X. Mi, X. Zheng, Q. Sun, J. Du, Y. Zhang, Y. Qin, L. Chai, M. Zhu, Fretting behavior of oxide scale formed on ferritic/martensitic steel after pre-exposure to lead-bismuth eutectic, *Tribology International*, 2023, **185**, 108507, doi: 10.1016/j.triboint.2023.108507.

[67] Y. Cao, K. Hua, N. Li, Y. Tong, Y. Song, H. Wu, Q. Zhou, H. Wang, W. Liu, Revealing the critical failure factor and sub-surface damage mechanism of 316 stainless steel during fretting corrosion under the molten lead-bismuth eutectic, *Tribology International*, 2023, **187**, 108767, doi: 10.1016/j.triboint.2023.108767.

[68] I. V. Gorynin, G. P. Karzov, V. G. Markov, V. S. Lavrukhin, V. A.Yakovlev, Proceeding of Heavy Liquid-Metal Coolants in Nuclear Technologies (HLMC-98), 1998, **1**, 120.

[69] K. Hua, Y. Cao, N. Li, Y. Tong, Y. Song, F. Zhang, X. Li, H. Wu, H. Wang, Revealing fretting corrosion synergistic mechanism of 316 stainless steel in liquid lead-bismuth eutectic (LBE), *Corrosion Science*, 2023, **215**, 111058, doi: 10.1016/j.corsci.2023.111058.

[70] J. F. Archard, Contact and rubbing of flat surfaces, *Journal of Applied Physics*, 1953, **24**, 981-988, doi: 10.1063/1.1721448.

[71] J. F. Archard, Single contacts and multiple encounters, *Journal of Applied Physics*, 1961, **32**, 1420-1425, doi: 10.1063/1.1728372.

[72] I.-M. Feng, H. H. Uhlig, Fretting corrosion of mild steel in air and in nitrogen, *Journal of Applied Mechanics*, 1954, **21**, 395-400, doi: 10.1115/1.4010939.

[73] I. R. McColl, J. Ding, S. B. Leen, Finite element simulation and experimental validation of fretting wear, *Wear*, 2004, **256**, 1114-1127, doi: 10.1016/j.wear.2003.07.001.

[74] K. Fallahnezhad, R. H. Oskouei, M. Taylor, Development of a fretting corrosion model for metallic interfaces using adaptive finite element analysis, *Finite Elements in Analysis and Design*, 2018, **148**, 38-47, doi: 10.1016/j.finel.2018.05.004.

[75] H. Mohrbacher, B. Blanpain, J. P. Celis, J. R. Roos, Low amplitude oscillating sliding wear on chemically vapour deposited diamond coatings, *Diamond and Related Materials*, 1993, **2**, 879-884, doi: 10.1016/0925-9635(93)90243-U.

[76] H. Mohrbacher, B. Blanpain, J. P. Celis, J. R. Roos, The influence of humidity on the fretting behaviour of PVD TiN coatings, *Wear*, 1995, **180**, 43-52, doi: 10.1016/0043-1648(94)06538-1.

[77] H. Mohrbacher, B. Blanpain, J. P. Celis, J. R. Roos, L. Stals, M. Van Stappen, Oxidational wear of TiN coatings on tool steel and nitrided tool steel in unlubricated fretting, *Wear*, 1995, **188**, 130-137, doi: 10.1016/0043-1648(95)06637-3.

[78] S. Fouvry, P. Kapsa, L. Vincent, Fretting behaviour of hard coatings under high normal load, *Surface and Coatings Technology*, 1994, **68**, 494-499, doi: 10.1016/0257-8972(94)90207-0.

[79] S. Fouvry, P. Kapsa, L. Vincent, Analysis of sliding behaviour for fretting loadings: determination of transition criteria, *Wear*, 1995, **185**, 35-46, doi: 10.1016/0043-1648(94)06582-9.

[80] S. Fouvry, P. Kapsa, L. Vincent, Quantification of fretting damage, *Wear*, 1996, **200**, 186-205, doi: 10.1016/S0043-1648(96)07306-1.

[81] C. Paulin, S. Fouvry, C. Meunier, Finite element modelling of fretting wear surface evolution: Application to a Ti–6A1–4V contact, *Wear*, 2008, **264**, 26-36, doi: 10.1016/j.wear.2007.01.037.

[82] K. Guo, C. Tian, Y. Wang, Y. Wang, W. Tan, An energy-based model for impact-sliding fretting wear between tubes and anti-vibration bars in steam generators, *Tribology International*, 2020, **148**, 106305, doi: 10.1016/j.triboint.2020.106305.

[83] G. Kai. An investigation on fretting wear mechanism and prediction model of steam generator tube bundles, PhD thesis, Tianjin University, Tianjin, China, 2020.

[84] S. Pan, C. Li, T. Jia, Y. Wang, An improved energy wear model of three-dimensional ball-plane contact structure and its fretting wear dynamic behaviors study, *Wear*, 2024, **550**, 205405, doi: 10.1016/j.wear.2024.205405.

[85] S. Huang. Numrical Analysis of Tangential Fretting Wear Based on Rough Surface. Master thesis, Southwest Jiaotong University, Xian, China, 2017.

[86] L. Li, H. Tian, Q. Yun, W. Chu, Study on temperature rise distribution of contact surface under cyclic load, *Proceedings of the Institution of Mechanical Engineers, Part J: Journal of Engineering Tribology*, 2021, **235**, 138-148, doi: 10.1177/1350650120919877.

[87] L. Li, W. Zhang, G. Li, J. Wang, L. Li, M. Xie, Simulation study of thermal–mechanical coupling fretting wear of Ti-6Al-4V alloy, *Applied Sciences*, 2022, **12**, 7400, doi: 10.3390/app12157400.

[88] Y. Y. Luo, Y.P. Wang, Z.H. Sun, H. Liang. Ultrasonic Recognition and Performance Degradation Model of Electrical Connector Fretting Wear. *China Mechanical Engineering*, 2023, **34,** 164-171.

[89] D. Zhang., S. Ge.. Research on the Evaluation Parameters and Theory Model of Fretting Wear between Steel Wires, *Tribology*, 2005, **25**, 50-54.

[90] P. H. Shipway, A. M. Kirk, C. J. Bennett, T. Zhu,

Understanding and modelling wear rates and mechanisms in fretting *via* the concept of rate-determining processes - Contact oxygenation, debris formation and debris ejection, *Wear*, 2021, **486**, 204066, doi: 10.1016/j.wear.2021.204066.

[91] Y. Zhong, W. Zhang, Q. Chen, J. Yang, C. Zhu, Q. Li, J. Yang, N. Liu, J. Yang, Effect of LBE corrosion on microstructure of amorphous Al_2O_3 coating by magnetron sputtering, *Surface and Coatings Technology*, 2022, **443**, 128598, doi: 10.1016/j.surfcoat.2022.128598.

[92] H. Glasbrenner, F. Gröschel, Exposure of pre-stressed T91 coated with TiN, CrN and DLC to Pb–55.5Bi, *Journal of Nuclear Materials*, 2006, **356**, 213-221, doi: 10.1016/j.jnucmat.2006.05.038.

[93] H. Rui, H. P. Zhu, F. L. Niu, Y. G. Zhao, Y. Zhang, A. X. Yang, T. Zhou, Effect of LBE corrosion on surface wettability of Ti_3SiC_2 at 450°C, *Materials Science Forum*, 2019, **944**, 458-465, doi: 10.4028/www.scientific.net/msf.944.458.

[94] E. Miorin, F. Montagner, V. Zin, D. Giuranno, E. Ricci, M. Pedroni, V. Spampinato, E. Vassallo, S. M. Deambrosis, Al rich PVD protective coatings: a promising approach to prevent T91 steel corrosion in stagnant liquid lead, *Surface and Coatings Technology*, 2019, **377**, 124890, doi: 10.1016/j.surfcoat.2019.124890.

[95] A. Weisenburger, A. Heinzel, G. Müller, H. Muscher, A. Rousanov, T91 cladding tubes with and without modified FeCrAlY coatings exposed in LBE at different flow, stress and temperature conditions, *Journal of Nuclear Materials*, 2008, **376**, 274-281, doi: 10.1016/j.jnucmat.2008.02.026.

[96] Q. Li, Y. Zhong, W. Zhang, H. Liu, J. Yang, C. Zhu, J. Deng, S. Zhao, Y. Zhong, M. Zhou, X. Qiu, J. Yang, Microstructure, mechanical properties, and lead–bismuth eutectic corrosion behaviors of FeCrAlY-Al_2O_3 nanoceramic composite coatings, *Coatings*, 2024, **14**, 393, doi: 10.3390/coatings14040393.

[97] W. Zhang, M. Zhou, Y. Fu, X. Qiu, J. Yang, Effect of sputtering bias voltage on the microstructure and lead-bismuth eutectic corrosion resistance of the FeCrAlY coating, *Corrosion*, 2024, **80**, 444-454, doi: 10.5006/4509.

[98] J. Yang, K. Shi, W. Zhang, Q. Chen, Z. Ning, C. Zhu, J. Liao, Y. Yang, N. Liu, W. Zhang, J. Yang, A novel AlCrFeMoTi high-entropy alloy coating with a high corrosion-resistance in lead-bismuth eutectic alloy, *Corrosion Science*, 2021, **187**, 109524, doi: 10.1016/j.corsci.2021.109524.

[99] J. Yang, L. Lyu, X. Qiu, M. Zhou, Y. Zhou, Q. Li, Q. Chen, H. Liu, Y. Zhong, J. Deng, W. Zhang, C. Zhu, N. Liu, J. Yang, Improved lead-bismuth eutectic corrosion resistance and mechanical properties of reactive gas pulse sputtered AlCrFeMoTi/(AlCrFeMoTi)N composite multilayered high-entropy alloy coatings, *Journal of Nuclear Materials*, 2022, **572**, 154093, doi: 10.1016/j.jnucmat.2022.154093.

[100] E. Serag, B. Caers, P. Schuurmans, S. Lucas, E. Haye, Challenges and coating solutions for wear and corrosion inside Lead Bismuth Eutectic: a review, *Surface and Coatings Technology*, 2022, **441**, 128542, doi: 10.1016/j.surfcoat.2022.128542.

[101] R. V. Umretiya, B. Elward, D. Lee, M. Anderson, R. B. Rebak, J. V. Rojas, Mechanical and chemical properties of PVD and cold spray Cr-coatings on Zircaloy-4, *Journal of Nuclear Materials*, 2020, **541**, 152420, doi: 10.1016/j.jnucmat.2020.152420.